Journal of Hydrology: Regional Studies 13 (2017) 168–188

Contents lists available at ScienceDirect

Journal of Hydrology: Regional Studies

journal homepage: www.elsevier.com/locate/ejrh

The influence of water/rock − water/clay interactions and mixing in the salinization processes of groundwater

Julien Walter[a,*], Romain Chesnaux[a], Vincent Cloutier[b], Damien Gaboury[a]

[a] Centre d'études sur les ressources minérales, Groupe de recherche R2eau, Département des sciences appliquées, Université du Québec à Chicoutimi, Saguenay, Québec, Canada, Canada

[b] Groundwater Research Group, Institut de recherche en mines et en environnement, Université du Québec en Abitibi-Témiscamingue, Campus d'Amos, Amos, Québec, Canada

ARTICLE INFO

Keywords:
Hydrogeochemistry
Groundwater salinization
Precambrian shield
Granular deposits
Multivariate analysis

ABSTRACT

Study region: Groundwater from the Precambrian Shield rock and Pleistocene deposit aquifers in Saguenay-Lac-Saint-Jean region (> 13 000 km^2) in the province of Quebec, Canada.

Study focus: Interpretations are based on the combination of *hierarchical cluster analysis* (HCA) results, *principal component analysis* (PCA), binary plots investigations ([Na^+, Ca^{2+}, Br^-] *vs.* Cl^-; Ca^{2+} *vs.* HCO_3^-; Ca^{2+} *vs.* Na^+) and Piper diagram investigations. The HCA and PCA was applied on 321 samples to specifically enable the identification of two very distinct salinization paths that produce the brackish groundwater in the study area.

New hydrological insights for the region: The results show that each of the two salinization paths exerts a major and different influence on the chemical signature of groundwater. Groundwater present in the crystalline bedrock naturally evolve from a recharge-type groundwater (Ca-HCO_3-dominant) to a type of brackish groundwater (Ca-(Na)-Cl-dominant) due to water/rock interactions (plagioclase weathering and mixing with deep basement fluids). Groundwater evolution in confined aquifers is dominated by water/clay interactions. The term water/clay interactions was introduced in this paper to account for a combination of processes: ion exchange and/or leaching of salt water trapped in the regional aquitard. Mixing with fossil seawater might also increase the groundwater salinity. PCA revealed that Ca^{2+}, Sr^{2+}, Ba^{2+} are highly correlated with groundwater from bedrock aquifers, while Mg^{2+}, SiO_2, K^+, $SO_4^{2-}$and HCO_3^- are more representative of the regional confining conditions.

1. Introduction

Deep groundwater in crystalline basement is typically highly mineralized, as indicated by numerous studies (Edmunds et al., 1984; Frape and Fritz, 1987; Fritz et al., 1994; Gascoyne and Kamineni, 1994; Lodemann et al., 1997; Bucher and Stober, 2010). Saline to brine waters are systematically encountered deep in the crust by 1) nuclear waste disposal programs in various countries, particularly in Canada (Gascoyne et al., 1995), Sweden (Nordstrom et al., 1989), Finland (Lahermo and Lampen, 1987), and Switzerland (Pekdeger and Balderer, 1987); in continental deep drilling programs (Russia: Kola island well; Germany: KTB); and in geothermal energy programs (France: Soultz-sous-Forêts; Switzerland: Urach; U.K.: Cornwall; USA: Los Alamos). Brackish to highly saline brines have been detected at depths down to several kilometers in many mines in crystalline rocks, particularly in the Canadian Shield (Fritz and Frape, 1982; Frape and Fritz, 1987) and in oil field sedimentary basins around the world (Fyfe et al., 1978; Kharaka

* Corresponding author.
E-mail address: julien_walter@uqac.ca (J. Walter).

http://dx.doi.org/10.1016/j.ejrh.2017.07.004
Received 3 January 2017; Received in revised form 3 June 2017; Accepted 24 July 2017
2214-5818/ © 2017 The Authors. Published by Elsevier B.V. This is an open access article under the CC BY-NC-ND license (http://creativecommons.org/licenses/BY-NC-ND/4.0/).

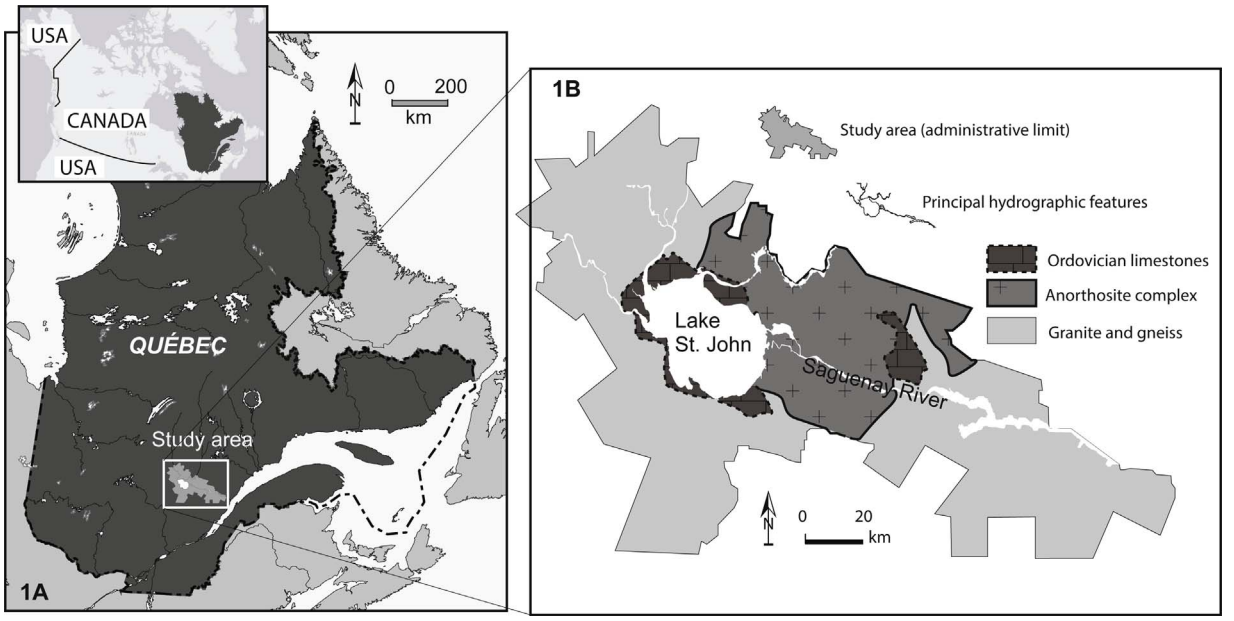

Fig. 1. A. Location of the study area and B, conceptual model of the geological features (adapted from CERM-PACES, 2013).

and Hanor, 2003). Overall, the water from basement rocks is systematically contaminated with brines at depths of less than 5 km (Pauwels et al., 1993; Bucher and Stober, 2010).

New chemical and isotopic data have yielded several hypotheses to explain the occurrence of saline groundwater deep in the crust. Total dissolved solids (TDS) generally increase with depth, and chlorides are the common salts. According to Bucher and Stober (2010), this chlorinity probably has a common global source because it is present at depth in all continental basement units worldwide. The main theories about the origins of the brines in Precambrian Shields include: 1) modified Paleozoic seawater (Bottomley et al., 1994) or basinal brines (Guha and Kanwar, 1987); 2) leaching of saline fluid inclusions in crystalline rocks (Nordstrom and Olsson, 1987); and 3) intense water/rock interactions (Frape and Fritz, 1987; Gascoyne et al., 1987; Kamineni, 1987; Bucher and Stober, 2010). More recently, studies on glaciation effects have demonstrated that glacial meltwater infiltrating bedrock aquifers has a major impact on groundwater chemistry (Lemieux et al., 2008; Aquilina et al., 2015; McIntosh et al., 2011). Clearly, a combination of several different physicochemical processes rather than a single process appears responsible for the generation of basement water (Douglas et al., 2000; Frape et al., 2003; Bucher et al., 2012). Studies of the origin and evolution of fluids in crystalline rocks are ongoing and are constantly being supplemented by new data contrasting geochemical conditions at different study sites.

Brackish groundwater have been identified at shallow depths (< 100 m) in fractured rock aquifers and in Pleistocene granular aquifers in the Saguenay-Lac-Saint-Jean region (SLSJ) in the province of Quebec, Canada (Fig. 1) by Dessureault (1975) and Walter (2010). In the study area, bedrock mainly consists of a variety of igneous and metamorphic Precambrian Shield rocks and some Ordovician remnants of several units of sedimentary rocks (shale, limestone and siltstone). The rocks of the basement are cut by a Phanerozoic faulted graben that defines the limits between the highlands and lowlands. Based on the specific morphology of the graben in the SLSJ region, a discharging regional gravity-driven flow system according to the Tóth model (Tóth, 1999) would explain the natural contamination by salt of lower fresh groundwater systems in the lowlands (Walter, 2010). The lowlands are covered by highly heterogeneous surficial Pleistocene deposits that include a semi-continuous regional aquitard of marine origin left behind by the retreat of seawater approximately 10,000 years ago (Lasalle and Tremblay,1978). The leaching of trapped salt in the regional marine clay confining layer would explain the presence of brackish groundwater in some confined Pleistocene aquifers in the SLSJ region (Dessureault, 1975).

Groundwater quality has major implications for drinking water and other groundwater uses, such as agriculture and manufacturing. The SLSJ region is a perfect laboratory field for testing the hypotheses of groundwater salinization for the following reasons: 1) a large hydrogeological database, including hydrogeochemical data, covering the entire region is available; 2) the graben topography implies that all surficial waters are drained toward the lowlands, thus defining a single watershed; 3) various aquifer types are known.

This study is based on a regional-scale dataset of 321 samples. The initial purpose of the sampling was to characterize the groundwater quality and the possible exposition of the local population to natural and/or anthropic contaminants (CERM-PACES, 2013). Therefore, sampling was conducted on existing private wells, usually used for drinking water supply. The physical characteristics of the sampling wells (location of the well screen, geology of the aquifer, casing depth) are poorly documented. Based on this regional database, this paper is a first attempt to statistically characterize groundwater chemistry in the SLSJ region with the goal of deciphering the possible geochemical evolution of groundwater controlled by the process of salinization. Another objective is to

test whether this evolution is similar within two different types of aquifers: fractured rock and porous granular sediments.

Multivariate analyses are performed on the regional-scale dataset of 321 samples and the results are discussed by means of graphical representations (log–log plot, Piper plot). Based on the existing literature, chemical reactions are proposed to explain the chemical trends observed in the data. In the SLSJ region, the groundwater dynamic appears to be largely influenced by the topography of the graben that is responsible for influencing the local discharge of contaminated groundwater (brines) from the deep crust involving natural cross-contamination issues.

2. Geology of the study area

The study area in the SLSJ region in the province of Quebec, Canada (Fig. 1A) covers 13,210 km^2, is oriented WNW-ESE and contains two important water bodies: Lake St. John (1200 km^2) and the Saguenay River (Fig. 1B), which is the main outlet of Lake St. John and is a tributary of the St. Lawrence River.

The following are the main geological features in the study area in chronological order:

1) Precambrian rocks of the Canadian Shield;
2) Ordovician limestone;
3) Pleistocene glacial drifts and fluvioglacial sediments;
4) Deep Pleistocene seawater deposits;
5) Pleistocene deltaic and shore deposits.

These features are described according to their chronostratigraphy in the following section.

2.1. Fractured rocks

The SLSJ region is located in the Allochthonous Polycyclic Belt (Rivers et al., 1989) in the Grenville Province of the Canadian Precambrian Shield (Laurin and Sharma, 1975). The main Precambrian lithologies are plutonic rocks that range in composition from felsic to intermediate and consist of a gneissic complex of orthogneiss and paragneiss (Hébert and Lacoste, 1998). One major event was the emplacement of the enormous Lac-Saint-Jean anorthosite complex and other intrusions between 1157 and 1142 Ma, covering an area of approximately 20,000 km^2 (Woussen et al., 1988; Hervet et al., 1994; Higgins and Van Breemen, 1996) (Fig. 1B).

A few remnants of an Ordovician platform composed of sedimentary rocks are found in the Lake St. John and Saguenay lowlands. These remnants form a series of stratified sedimentary rocks, including siliciclastic strata, micritic limestones and highly fossiliferous alternating limestones and shales (Desbiens and Lespérance, 1989). A maximum thickness of 110 m has been recorded in the Ordovician sequence by drilling in the Saguenay area (CERM-PACES, 2013). The limestones (Fig. 1B) occur along the northern, western and southern shores of the lake and are separated from the Saguenay outcrops by approximately 45 km of Precambrian rocks (Kénogami uplands).

2.2. Bedrock topography

The bedrock that controls the topography is cut by the Phanerozoic Saguenay Graben that is approximately 30 km wide and is crossed by a NNE-SSW rise in the elevation of the bedrock (*Kénogami uplands*; Fig. 2, model B). The northern and southern walls of the Saguenay Graben are bounded by WNW fault systems (Du Berger et al., 1991) that mark the limits between the lowlands (from 0 m to approximately 200 m above the sea level) and the highlands (up to 1000 m above sea level). Outcrops with rugged terrain dominate the highlands (Fig. 2, model C), whereas the topography of the lowlands is relatively flat due to the important local accumulations of Pleistocene deposits having a thickness of up to 180 m (CERM-PACES, 2013; Fig. 2, model A).

The geological structures along the western side of the study area are oriented NNW-SSE (Fig. 2; model A). In the northwestern portion of the study area, the delimitation between the highlands and the lowlands is not clear, thus giving an asymmetrical shape to the topography from north to south (half graben system, Fig. 2). Remnants of Ordovician limestone units have been identified principally in the lowlands (Fig. 2, model A), mostly at the border of the Lake St. John. Limestones are generally covered by sequences of Pleistocene deposits.

2.3. Pleistocene deposits

In North America, the last glaciation began approximately 85,000 years ago during the early stage of the Wisconsinan period and ended approximately 7000 years ago (Parent and Occhietti, 1988). During its retreat toward the west-northwest (orientation of the graben), the last glacier covering the region left a discontinuous and heterogeneous layer of till, several terminal moraines, glaciolacustrine deposits and important fluvioglacial esker deposits (Daigneault et al., 2011 LaSalle and Tremblay, 1978). The morphology of the graben in the study area controlled the local accumulation of up to 50 m of interbedded sand and coarse grain fluvioglacial sediments (CERM-PACES, 2013; Fig. 2, models A, B and C).

After the retreat of the glacier, the lowlands in the area were invaded approximately 10,000 years ago by the Laflamme Sea (Dionne and Laverdière, 1969). This invasion resulted in a semi-continuous extensive layer of deep-water sediments consisting of laminated argillaceous silt and grey silty clay (Tremblay, 1971; LaSalle and Tremblay, 1978). The fine-grained sea deposits contain

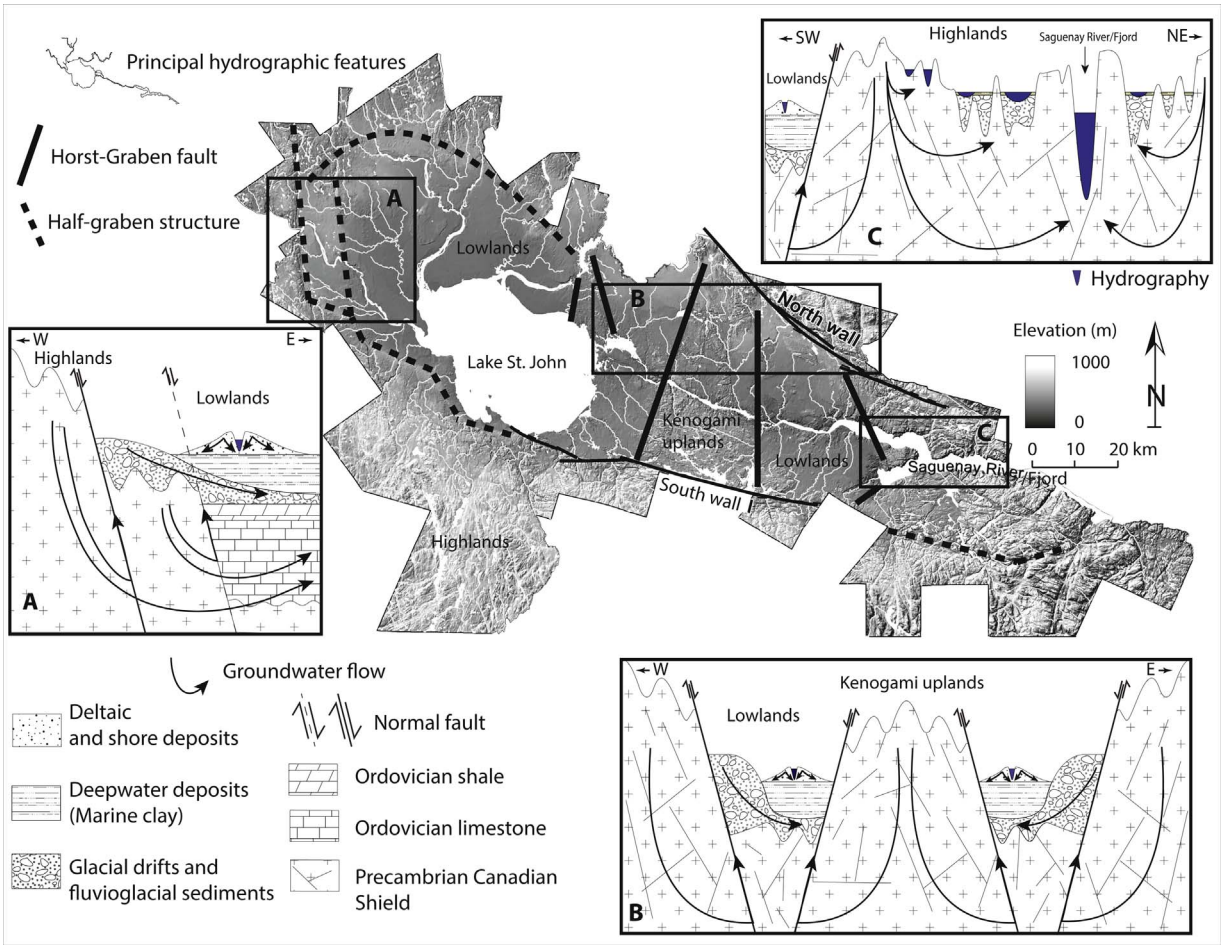

Fig. 2. Schematic of regional A, graben topography, B, major hydrogeological features and C, general flow lines.

salty interstitial water (Bouchard et al., 1983) and are relatively abundant, with a thickness of up to 100 m in some areas within the limits of the graben (Dessureault, 1975; Fig. 2, models A, B and C). The regional aquitard represents a confining layer for the underlying aquifers (Dessureault, 1975; CERM-PACES, 2013).

The isostatic uplift in response to the long-term subsidence of the region due to the weight of ice-forced the retreat of the Laflamme Sea (Bouchard et al., 1983; Lasalle and Tremblay, 1978). At that time, various facies of deltaic, littoral and pre-littoral sediments were emplaced on the top of the sedimentary sequences (Fig. 2, models A, B and C). These sediments are laminated with a highly heterogeneous stratigraphy, layers with particle sizes ranging from silt to gravel (Daigneault et al., 2011), and a thickness of up to 100 m (CERM-PACES, 2013).

2.4. Hydrogeological background

During the complex geological history of the SLSJ region, several hydrogeological environments have been created. Confined and/or unconfined aquifers occur in the fractured rock and Pleistocene deposits and combine locally to form multilayered aquifers (CERM-PACES, 2013), some of which are unconnected and some of which are interconnected (Chesnaux et al., 2012; Richard et al., 2014). Fluvioglacial sediments are the most productive regional aquifers. These aquifers are characterized by a hydraulic transmissivity (T) of 10^{-4} to 10^{-3} m^2/s and are consequently favored as a source of municipal drinkable water (CERM-PACES, 2013). These reservoirs are frequently covered by the regional marine clay aquitard (Dessureault, 1975; CERM-PACES, 2013) but can also be unconfined, particularly in the major valleys in the highlands that were not covered by the invading Laflamme Sea (Fig. 2, model C). Deltaic and shore deposits exhibit variable T values ranging from 10^{-5} m^2/s to 10^{-2} m^2/s. These sediments constitute the major regional water-table aquifers (CERM-PACES, 2013).

Fractured rock aquifers exhibit relatively low values of T (10^{-6} to 10^{-5} m^2/s), with local maximum values of 10^{-3} m^2/s attributed to regional-scale deformation zones (Hébert and Van Breemen, 2004; CERM-PACES, 2013). To date, no clear distinctions have been made between the hydraulic properties of Ordovician limestone and Precambrian rocks.

The regional hydrogeological flow systems can be divided into two major systems that characterize other graben topography

(Meinken and Stober, 1997). In the highlands, groundwater infiltrates into a network of interconnected fractures and faults within igneous and metamorphic rocks (Fig. 2, model A, B and C). In contrast, the regional water table in the lowlands replicates the topography (Fig. 2, model A, B and C). Lake St. John and the Saguenay River are the primary terminal discharge zones of the two regional groundwater flow systems.

2.5. Hydrogeochemical background

The groundwater in the study area exhibits a wide range of chemical compositions (Dessureault, 1975; Simard and Rosiers, 1979; Walter et al., 2006; Walter, 2010; Rouleau et al., 2011; Roy et al., 2011; Walter et al., 2011; CERM-PACES, 2013). Although the groundwater in the SLSJ area is largely of good quality, brackish groundwater and water with excessive trace element concentrations relative to Canadian drinking water quality guidelines (Health Canada, 2007), such as fluoride (> 1.5 mg/L), barium (> 1 mg/L), manganese (> 0.05 mg/L), iron (> 0.3 mg/L) and aluminum (> 0.1 mg/L), have recently been identified (CERM-PACES, 2013).

Simard and Des Rosiers (1979) presented an overview of several aquifers in the southern portion of Quebec. Among the 20 samples collected from the Precambrian bedrock in the SLSJ region, two occurrences of excessive fluoride content (> 1.5 mg/L), one excessive chloride concentration (> 250 mg/L), and one significant salinity value (> 1000 mg/L) were observed. According to Dessureault (1975), the marine clay regional aquitard is responsible for the presence of brackish groundwater in the confined Pleistocene sediments. Moreover, Walter (2010) identified brackish groundwater in the bedrock at shallow depths (< 100 m).

Walter (2010) suggests that the graben morphology of this region is responsible for the long residence time of the regional-scale flow system that discharges around Lake St. John (Fig. 2). The observations of Walter (2010) agree with the Tóth (1999) model, in which the salinity of groundwater increases with the scale of the flow system (i.e., local-scale (fresh groundwater), intermediate-scale (fresh to brackish groundwater), or regional-scale (brackish groundwater to brine)).

3. Methodology

3.1. Sampling sites and groundwater sampling locations

In this study, 363 samples were collected from private and municipal wells as part of two hydrogeochemical mapping campaigns in the SLSJ region. The first campaign was conducted in 2004 and 2005 and focused on brackish groundwater in the bedrock (Walter, 2010). The second campaign was conducted in 2010 and 2011 to establish an overview of the groundwater quality of the fractured rock and granular aquifers (CERM-PACES, 2013).

A conventional and recognized protocol was used to collect and preserve the samples (Cloutier et al., 2006; Walter, 2010; Montcoudiol et al., 2013; Ghesquière et al., 2015). The chemical analyses were performed in certified laboratories using standard methods (Table 1). The sampling protocol included follow-up of selected physicochemical parameters when purging the wells (temperature; redox potential, Eh; pH; dissolved oxygen; and electrical conductivity; Table 1). Purging was complete when the physicochemical parameters stabilized. The sampled water was filtered through a 0.45 μm filter and analyzed for major, minor and trace levels of 38 inorganic constituents (Table 1).

Among the 363 samples, 42 groundwater samples with an electro-neutrality beyond ± 10% were rejected (Hounslow, 1995; Appelo and Postma, 2005). Fig. 3 shows the locations of the remaining 321 groundwater sample sites used in this study. Among these samples, 170 and 151 samples were collected from bedrock and granular deposit aquifers, respectively.

3.2. Data processing

The proposed approach relies on a combination of: *hierarchical cluster analysis* (HCA), *principal component analysis* (PCA), binary plot investigations ($[Na^+, Ca^{2+}, Br^-]$ *vs.* Cl^-; Ca^{2+} *vs.* HCO_3^-; Ca^{2+} *vs.* Na^+) and Piper diagram interpretations. HCA is applied with the objective of grouping end-member samples according to their chemical similarities. PCA is next applied to the same subset to reveal details relating to end-member chemistry. All samples from the regional dataset are plotted on binary plots and a Piper diagram to highlight groundwater chemical evolution. The data processing methods used to determine the geochemical characteristics of the samples and the evolution of the water are presented in the following sections as steps 1 through 3.

3.2.1. Step 1: selection of the chemical elements used in multivariate analysis

Censored data are not appropriate for many multivariate statistical techniques (Güler et al., 2002). Therefore, the non-detected, less-than, and greater-than values must be replaced by unqualified values (Farnham et al., 2002). When dealing with below detection limit (DL) or DL values for a given dataset, Farnham et al. (2002) showed that substitution with DL/2 gave better results than using DL or 0. Therefore, to prevent sample exclusion, we replaced DL concentrations by half the value of the detection limit (DL/2).

Irrelevant performances of all substitution methods have been obtained when the number of ' < DL' values exceeded approximately 25% of the dataset (Farnham et al., 2002). For this reason, chemical parameters were selected with the aim of having less than 25% censored data.

3.2.2. Step 2: multivariate statistical analysis

Multivariate analyses are designed to highlight the linear correlations between variables and they assume that the values of the variables satisfy a normal statistical distribution (Brown, 1998). The Box-Cox power transformation was applied to the regional data

Table 1
Summary statistical data for the 321 samples.

	N	Mean	Median	Min	Max	25	75	% det	Multivariate
TDS (mg/L)	321	611.8	280.4	12.1	8266.6	153.5	467.9	100%	–
Temperature (Celcius)[a]	317	8.1	7.6	4.0	15.6	7.0	8.8	99%	–
Redox potential (mV)[a]	283	49.0	82.9	−375.6	743.9	−21.2	108.4	88%	–
pH[a]	318	7.7	7.5	4.4	10.8	6.5	8.1	99%	–
Dissolved oxygen (mg/L)[a]	275	2.8	0.7	0.0	90.0	0.0	4.1	86%	–
Bicarbonates[e]	**321**	**162.3**	**146.4**	**6.1**	**695.4**	**76.3**	**219.6**	**100%**	**x**
Silicium[b]	**321**	**6.2**	**5.7**	**0.220**	**16.0**	**4.8**	**7.3**	**100%**	**x**
Sodium[b]	**320**	**116.7**	**14.0**	**0.870**	**2500.0**	**3.7**	**74.8**	**100%**	**x**
Calcium[b]	**319**	**62.0**	**26.0**	**0.040**	**1500.0**	**10.0**	**58.0**	**99%**	**x**
Potassium[b]	**318**	**4.6**	**2.1**	**0.120**	**82.0**	**1.0**	**4.3**	**99%**	**x**
Magnesium[b]	**317**	**10.5**	**4.3**	**0.021**	**220.0**	**1.7**	**9.7**	**99%**	**x**
Chloride[c]	**317**	**212.9**	**10.0**	**0.160**	**4200.0**	**2.3**	**64.5**	**99%**	**x**
Strontium[b]	**317**	**1.5**	**0.2**	**0.003**	**37.0**	**0.1**	**0.7**	**99%**	**x**
Sulfates[c]	**316**	**31.2**	**11.0**	**0.200**	**530.0**	**4.8**	**20.0**	**98%**	**x**
Barium[b]	**303**	**0.103**	**0.041**	**0.003**	**2.800**	**0.018**	**0.090**	**94%**	**x**
Aluminium[b]	**292**	**0.014**	**0.007**	**0.001**	**0.230**	**0.004**	**0.014**	**91%**	**x**
Manganese[b]	**285**	**0.079**	**0.017**	**0.000**	**2.400**	**0.004**	**0.064**	**89%**	**x**
Zinc[b]	**260**	**0.035**	**0.014**	**0.002**	**0.710**	**0.008**	**0.031**	**81%**	**x**
Boron[b]	**250**	**0.150**	**0.046**	**0.004**	**3.400**	**0.013**	**0.180**	**78%**	**x**
Fluoride[d]	234	0.923	0.700	0.060	4.900	0.300	1.500	73%	–
Amonium[d]	227	0.253	0.080	0.020	5.700	0.040	0.230	71%	–
Copper[b]	213	0.014	0.004	0.001	0.350	0.002	0.013	66%	–
Lead[b]	203	0.001	0.000	0.000	0.010	0.000	0.001	63%	–
Iron[b]	173	1.051	0.120	0.002	35.000	0.048	0.370	54%	–
Molybdene[b]	171	0.003	0.002	0.001	0.024	0.001	0.003	53%	–
Nitrate[c]	136	0.896	0.300	0.020	8.600	0.100	1.075	42%	–
Silver[b]	85	0.0004	0.0002	0.0001	0.0090	0.0001	0.0003	26%	–
Nickel[b]	82	0.003	0.002	0.001	0.020	0.001	0.003	26%	–
Bromide[c]	75	6.565	2.500	0.100	45.000	0.700	11.000	23%	–
Lithium[b]	72	0.038	0.015	0.001	0.570	0.010	0.036	22%	–
Uranium[b]	59	0.004	0.002	0.001	0.020	0.001	0.004	18%	–
Chromium[b]	46	0.001	0.001	0.001	0.011	0.001	0.001	14%	–
Vanadium[b]	18	0.003	0.003	0.002	0.007	0.002	0.003	6%	–
Inorganic phosphorus[d]	16	0.154	0.070	0.040	0.500	0.050	0.260	5%	–
Cobalt[b]	15	0.002	0.001	0.001	0.007	0.001	0.003	5%	–
Antimony[b]	9	0.002	0.002	0.001	0.005	0.001	0.003	3%	–
Cadmium[b]	9	0.000	0.000	0.000	0.001	0.000	0.001	3%	–
Tin[b]	3	0.002	0.002	0.001	0.003	0.001	–	1%	–
Titanium[b]	3	0.002	0.001	0.001	0.004	0.001	–	1%	–
Beryllium[b]	2	0.003	0.003	0.001	0.004	0.001	–	1%	–
Selenium[b]	1	0.042	0.042	0.042	0.042	0.042	0.042	0%	–
Bismuth[b]	1	0.001	0.001	0.001	0.001	0.001	0.001	0%	–

ANALYTICAL METHODS.
For major, minor and trace elements, data are given in mg/L.
For the physical parameters, N = number of mesured data.
For the lab analysed parameters, N = Number of detected values.
If N = 1 or 2: data are underlined.
If N = 1: unique measured value is presented.
If N = 2: mean value is presented 25 and 75 header = the first and the third quantiles.
TDS is calculated using the software Aquachem v.5.0.
Multivariate header = parameters used in the multivariate analysis.
[a] multiparameter probe (in situ).
[b] Inductively Coupled Plasma Mass Spectrometry.
[c] Ionic chromatography.
[d] Specific probe.
[e] Titration.

set to represent the data as a normal distribution (Box and Cox, 1964; ArandaCirerol et al., 2006). Each of the selected variables (in major, minor and trace elements) were then standardized to unit variance. The standardized data were obtained for each element by subtracting the mean concentration of the element from each concentration and dividing by the standard deviation of the distribution (Davis, 2002). At that point, the values for each element were measured in standard deviation units, and the multivariate analysis could be performed. The software Statistica version 6.1 (Statsoft Inc., Ok, USA; 2013) was used to perform the multivariate statistical analysis.

3.2.2.1. Hierarchical cluster analysis. Hierarchical cluster analysis (HCA) is used to identify the optimal clustering in which the

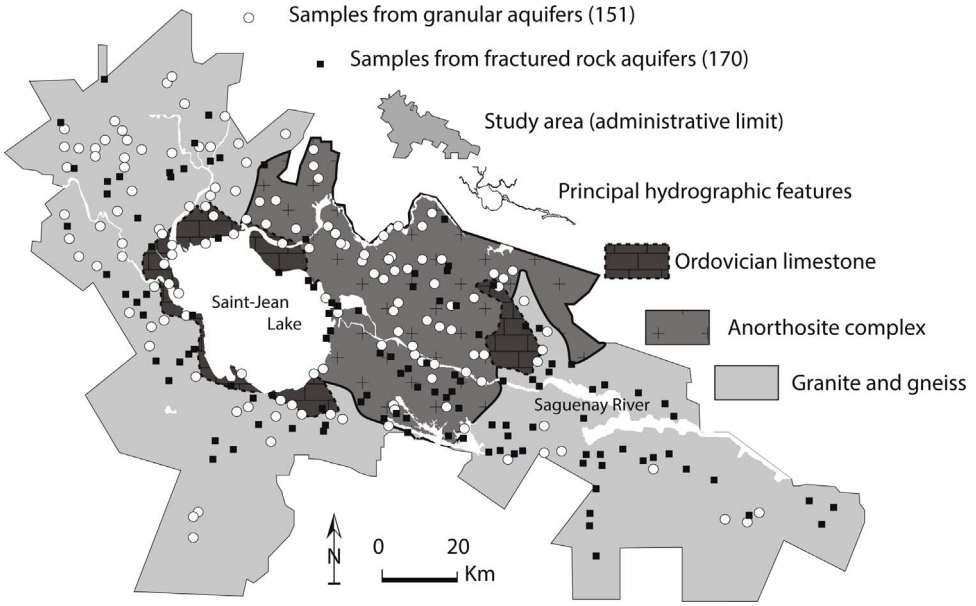

Fig. 3. Location of the 321 groundwater sample sites in this study.

groundwater samples within each cluster are geochemically similar and the different clusters are geochemically dissimilar (Alvin, 2002). When applying HCA to the regional data set, the clusters that are obtained correspond to samples exhibiting similar geochemical characteristics. Consequently, the HCA produced different cluster samples, each characterized by particular chemical contents. In this manner, HCA helps to define chemical end-members of different origins within the study area. Specifically, the Euclidian distance as a distance measure of similarities and Ward's method as a linkage rule are the best combination for producing the most distinctive groups when applied to groundwater chemical analysis (Güler et al., 2002; Cloutier et al., 2008; Templ et al., 2008).

3.2.2.2. Principal component analysis. Principal component analysis (PCA) was used with the aim of reducing and deciphering patterns within the large set of water chemistry data into principal components (PC). PC are expressed as linear functions of the chemical elements and the emphasis is on explaining the total variance of the subset of samples. We present PCA results on two different plots commonly referred to as *correspondence circle graphs*. In one graph, PCA values plot chemical element loadings while the second plots the sample scores.

3.2.3. Step 3: graphical representations of the investigations

3.2.3.1. Binary diagrams. Investigations of salinization processes typically rely on log–log plots of Na^+, Ca^{2+} and Br^- concentrations *vs.* Cl^- concentrations. Chloride (Cl^-) plays a predominant role in groundwater salinization (Chebotarev, 1955; Tóth, 1985; Cloutier et al., 2010). Because seawater is the major source of Cl^- on Earth, the composition of groundwater is frequently compared with the composition of seawater to discuss the origin of salinity and, more specifically, the possibility of mixing between dilute freshwater and a seawater end-member (Frape and Fritz, 1987). Moreover, many authors used this comparison to discuss the water/rock interaction control of saltwater chemistry (Frape and Fritz, 1987; Beaucaire et al., 1999; Walter, 2010). Geochemically conservative elements such as bromide (Br^-) are particularly relevant and useful for investigating salinization processes (Edmunds et al., 1985; Bottomley et al, 1999; Cloutier et al., 2010).

3.2.3.2. Piper diagram. As most of the interpretations presented in this paper are based on the major chemical elements of groundwater (Ca^{2+}, Na^+, Cl^-, HCO_3^-), the chemical results can be plotted on a Piper diagram (Piper, 1944) to interpret general geochemical evolution pathways of groundwater in the study area. Piper diagrams are widely used in the literature to illustrate trends in the chemical evolution of groundwater based on chemical facies.

4. Results

Summary statistics regarding the chemical contents of the regional data set are presented in Table 1. The chemistry of the individual 321 samples is presented in the Supplementary Material (see the electronic appendix). Table 1 presents the number of analyses with values above the detection limit (*N*), the mean, the median, the first (*25*) and third (*75*) quartiles, the maximum (*Max)* and the minimum (*Min*) values. The frequency of detection is calculated for each physicochemical parameters and is presented in Table 1 (% value). The frequency of detection corresponds to the percentage of *N* over the 321 samples of the dataset (% value = (*N*/

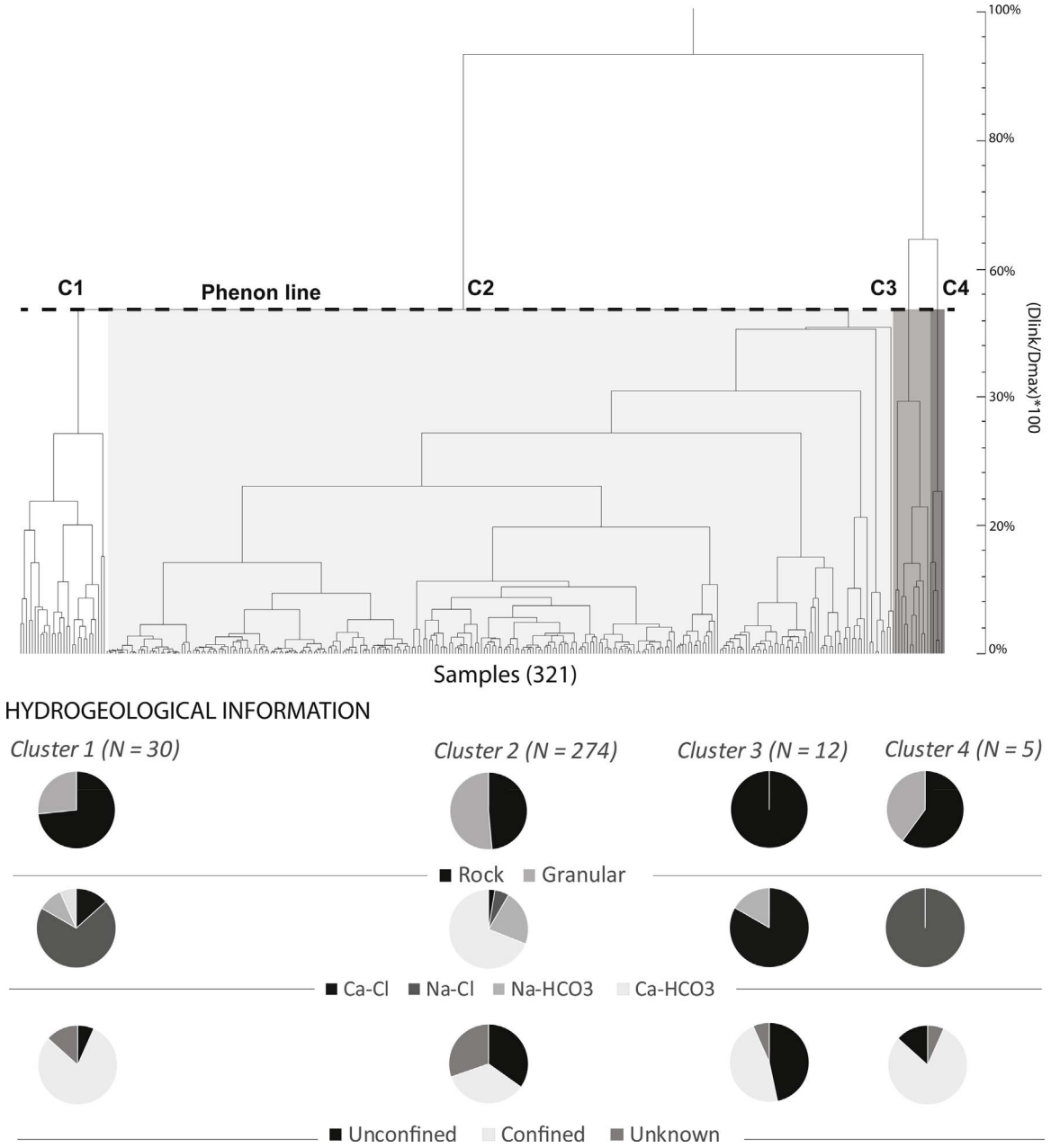

Fig. 4. Dendrogram produced from hierarchical cluster analysis. When Dlink is < 60% of Dmax (i.e., position of the Phenon line), the samples are divided into four clusters (C1 to C4).

321) × 100)). The chemical parameters for which the frequency of detection was > 75% were used to perform the multivariate analyses. The selected parameters are marked in Table 1 using bold characters and checked in Table 1 (column *Multivariate*).

4.1. Hierarchical cluster analysis

HCA determined the levels of similarity for samples and presented the results in a dendrogram (Fig. 4). The number of clusters increases when the position of the Phenon line is moved from top to bottom on the dendrogram. Owing to this subjective evaluation, HCA is a semi-objective method (Güler et al., 2002). For this study, four clusters provided the most satisfactory result. Descriptive statistics, the water and aquifer types for each cluster are presented in Table 2.

The largest cluster is Cluster 2 (N = 274) mainly composed of Ca(Na)-HCO_3 samples (251/274). Almost half of these samples come from unconfined environments (127/274), and for around 25% of the Cluster 2 samples, the hydrogeological context is unknown (67/274). The median depth for Cluster 2 is 36 m, the shallowest median depth of all clusters. Chloride waters (calcium and

Table 2
Water type, aquifer type, median depth of the sample wells and chemical content (median) of the four clusters obtained by hierarchical cluster analysis (HCA).

	Cluster 1 (N = 30)			Cluster 2 (N = 274)			Cluster 3 (N = 12)			Cluster 4 (N = 5)		
Water type	Na-Cl (21) / Ca-Cl (4)			Na-Cl (16) / Ca-Cl (7)			Na-Cl (2) / Ca-Cl (10)			Na-Cl (5) / Ca-Cl (0)		
	Na-HCO3 (3) / Ca-HCO3 (2)			Na-HCO3 (62) / Ca-HCO3 (189)			Na-HCO3 (0) / Ca-HCO3 (0)			Na-HCO3 (0) / Ca-HCO3 (0)		
Aquifer type	Rock (22) / Granular (8)			Rock (133) / Granular (141)			Rock (12) / Granular (0)			Rock (3) / Granular (2)		
Hydrogeological Context[a]	UnC (2) / C (24) / UnK (4)			UnC (127) / C (77) / UnK (67)			UnC (4) / C (7) / UnK (1)			UnC (1) / C (4) / UnK (0)		
PARAMETER	Min	Med	Max	Min	Med	Max	Min	Med	Max	Min	Med	Max
Depth (m)	0	59	127	0	36	198	64	106	153	8	69	105
TDS (mg/L)	575	1670	4197	12	233	1237	2113	2860	5228	5573	6301	8267
Temperature (Celcius)[b]	5.8	7.7	13.3	4.0	7.7	15.6	6.1	7.4	9.2	4.9	7.5	7.8
Redox potential (mV)[b]	−375.6	−22.1	108.2	−314.1	90.8	743.9	−258.5	−17.0	108.4	−100.0	−21.8	27.9
pH[b]	5.5	7.7	10.1	4.2	7.5	10.8	5.2	7.6	8.6	6.5	7.2	7.6
Dissolved oxygen (mg/l)[b]	0.0	0.0	9.9	0.0	1.2	90.0	0.0	0.1	0.4	0.0	0.0	1.8
Sodium	**20**	**430**	**1400**	**1**	**9**	**410**	**180**	**335**	**790**	**1600**	**1900**	**2500**
Magnesium	**0.04**	**15.80**	**79.00**	**0.02**	**3.60**	**26.00**	**3.00**	**47.00**	**96.00**	**100.00**	**160.00**	**220.00**
Potassium	**0.54**	**14.00**	**34.00**	**0.12**	**1.80**	**20.00**	**1.60**	**4.05**	**14.00**	**16.00**	**64.00**	**82.00**
Calcium	**0**	**58**	**310**	**0**	**23**	**170**	**210**	**665**	**1500**	**60**	**120**	**520**
Bicarbonates	**87**	**295**	**683**	**6**	**134**	**438**	**6**	**106**	**232**	**134**	**464**	**695**
Chloride	**29**	**590**	**2400**	**0**	**8**	**560**	**1000**	**1650**	**3000**	**2700**	**3200**	**4200**
Sulfates	**1**	**70**	**400**	**0**	**10**	**110**	**1**	**76**	**300**	**330**	**420**	**530**
Barium	**0.01**	**0.07**	**0.76**	**0.00**	**0.04**	**1.20**	**0.04**	**0.17**	**2.80**	**0.02**	**0.04**	**0.20**
Boron	**0.03**	**0.36**	**3.40**	**0.00**	**0.03**	**0.75**	**0.05**	**0.30**	**0.81**	**0.46**	**0.66**	**0.82**
Strontium	**0.003**	**1.550**	**9.100**	**0.014**	**0.170**	**4.300**	**11.000**	**18.500**	**37.000**	**1.400**	**3.700**	**27.000**
Silicium	**0.22**	**6.80**	**11.00**	**1.30**	**5.70**	**16.00**	**1.30**	**4.80**	**6.50**	**4.80**	**9.60**	**13.00**
Manganese	**0.0003**	**0.0355**	**0.1900**	**0.0004**	**0.0130**	**2.4000**	**0.0180**	**0.0855**	**0.7100**	**0.0430**	**0.0890**	**0.6100**
Fluoride	0.60	1.60	4.90	0.10	0.50	2.90	0.06	1.35	2.40	0.80	1.10	1.20
Aluminium	**0.002**	**0.007**	**0.087**	**0.001**	**0.007**	**0.230**	**0.004**	**0.010**	**0.026**	**0.0**	**0.009**	**0.020**
Bromide	0.43	2.93	19.44	0.10	0.51	5.96	13.82	19.23	45.00	10.00	12.00	19.00
Iron	0.005	0.150	3.100	0.002	0.115	35.000	0.008	0.093	17.000	0.190	1.000	1.300
Lithium	0.003	0.020	0.180	0.001	0.012	0.021	0.003	0.070	0.570	0.018	0.037	0.120
Zinc	**0.004**	**0.011**	**0.150**	**0.002**	**0.015**	**0.710**	**0.003**	**0.010**	**0.064**	**0.010**	**0.044**	**0.100**
Lead	0.0001	0.0002	0.0080	0.0001	0.0003	0.0073	0.0006	0.0080	0.0100	0.0080	0.0080	0.0080
Amonium	0.05	0.69	1.80	0.02	0.07	1.10	0.12	1.50	5.70	2.20	2.60	3.00
Copper	0.0008	0.0018	0.0070	0.0005	0.0050	0.3500	0.0006	0.0028	0.0220	0.0030	0.0030	0.0030
Molybdenium	0.0006	0.0033	0.0240	0.0005	0.0017	0.0180	0.0017	0.0059	0.0065	0.0014	0.0015	0.0150
Nickel	0.0009	0.0020	0.0098	0.0010	0.0018	0.0200	0.0009	0.0020	0.0020	0.0016	0.0018	0.0020
Silver	0.0001	0.0003	0.0090	0.0001	0.0002	0.0019	0.0002	0.0002	0.0002	0.0002	0.0002	0.0002
Uranium	0.0011	0.0019	0.0024	0.0010	0.0023	0.0200	< DL	< DL	< DL	0.0012	0.0016	0.0018
Chromium	0.0005	0.0008	0.0010	0.0005	0.0010	0.0110	0.0010	0.0010	0.0010	0.0005	0.0015	0.0024
Nitrate	0.40	0.43	0.46	0.02	0.30	8.60	< DL	< DL	< DL	< DL	< DL	< DL
Cobalt	< DL	< DL	< DL	0.0006	0.0014	0.0066	< DL	< DL	< DL	< DL	< DL	< DL
Inorganic phosphorus	0.05	0.08	0.11	0.04	0.14	0.50	0.06	0.06	0.06	0.04	0.04	0.04
Vanadium	< DL	< DL	< DL	0.0020	0.0026	0.0069	< DL	< DL	< DL	< DL	< DL	< DL
Antimony	< DL	< DL	< DL	0.0010	0.0016	0.0052	< DL	< DL	< DL	< DL	< DL	< DL
Cadmium	< DL	< DL	< DL	0.0002	0.0003	0.0007	< DL	< DL	< DL	< DL	< DL	< DL
Selenium	< DL	< DL	< DL	0.0420	0.0420	0.0420	< DL	< DL	< DL	< DL	< DL	< DL

(continued on next page)

Table 2 *(continued)*

	Cluster 1 (N = 30)			Cluster 2 (N = 274)			Cluster 3 (N = 12)			Cluster 4 (N = 5)		
Water type	Na-Cl (21) / Ca-Cl (4)			Na-Cl (16) / Ca-Cl (7)			Na-Cl (2) / Ca-Cl (10)			Na-Cl (5) / Ca-Cl (0)		
	Na-HCO3 (3) / Ca-HCO3 (2)			Na-HCO3 (62) / Ca-HCO3 (189)			Na-HCO3 (0) / Ca-HCO3 (0)			Na-HCO3 (0) / Ca-HCO3 (0)		
Aquifer type	Rock (22) / Granular (8)			Rock (133) / Granular (141)			Rock (12) / Granular (0)			Rock (3) / Granular (2)		
Hydrogeological Context[a]	UnC (2) / C (24) / UnK (4)			UnC (127) / C (77) / UnK (67)			UnC (4) / C (7) / UnK (1)			UnC (1) / C (4) / UnK (0)		
Tin	0.003	0.003	0.003	0.0011	0.0016	0.0021	< DL	< DL	< DL	< DL	< DL	< DL
Titanium	< DL	< DL	< DL	0.0010	0.0013	0.0044	< DL	< DL	< DL	< DL	< DL	< DL
Beryllium	< DL	< DL	< DL	0.0008	0.0026	0.0044	< DL	< DL	< DL	< DL	< DL	< DL
Bismuth	< DL	< DL	< DL	0.0007	0.0007	0.0007	< DL	< DL	< DL	< DL	< DL	< DL

For major, minor and trace elements, data are given in mg/L.
Under Detection Limit (< DL).
Non Applicable (NA).
Parameters presented in bold characters have been selected for multivariate treatment.
[a] Unconfined (UnC); Confined (C); Unknown (UnK).
[b] multiparameter probe (in situ); TDS is calculated using the software Aquachem v.5.0.

sodium type) are also found in Cluster 2. The chloride waters could not be clustered from the bicarbonate waters by moving downward the Phenon line on the dendrogram. In comparison to the other clusters, Cluster 2 represents a freshwater end-member. Cluster 2 also presents some samples representative of intermediate chlorinated facies situated between Cluster 2 and the other clusters (Clusters 1, 3 and 4) dominated by chloride.

Cluster 1 is mainly composed of Na(Ca)-Cl waters (25/30). The bicarbonate type samples of Cluster 1 dominate the other samples of Cluster 1 (5/30). Cluster 3 is exclusively composed of Ca(Na)-Cl (12/12) type samples, with a large predominance of Ca-Cl waters (10/12). Cluster 4 is the smallest cluster with only five samples (over the 321 samples of this study) which all are of Na-Cl type. Confined conditions dominate in Clusters 1, 3 and 4. The median depth for Cluster 1 is 59 m.

Cluster 4 shows the highest mean TDS value (median value = 6 301 mg/L as well as the highest minimum and maximum TDS values (respectively 5573 ppm and 8267 ppm). The median depth for Cluster 4 is 69 m. In Cluster 4, 3 samples were collected in bedrock aquifers and 2 samples were collected in granular aquifers. Confining conditions dominate Cluster 4. The TDS values are decreasing from Cluster 4 to Cluster 2 (Cluster 2 median value = 233 ppm). The mean TDS value of Cluster 3 (median = 2860 ppm) is almost the double as the one of Cluster 1 (Median = 1670 ppm). All the samples in Cluster 3 were collected in fractured rock aquifers. Cluster 3 has the greatest median depth value (106 m). Fractured rock aquifers also dominate in Cluster 1 (22/30). It must be underlined that this study does not address the issue of distinguishing water chemistry from Ordovician limestone and from the crystalline basement.

In Clusters 2 and 4, the numbers of samples from granular aquifers and the number of samples from fractured rock aquifers are almost the same. Based on HCA fundamentals, this observation suggests that brackish groundwater samples grouped in Cluster 3 and collected in the bedrock aquifers are chemically distinct from the brackish groundwater samples that are grouped in Clusters 1, 2 and 4.

4.2. Principal component analysis

To investigate the similarities/dissimilarities between clusters, the samples were plotted on the PCA correspondence circle according to the cluster to which they belong (Fig. 5A). The horizontal axis of the correspondence circle corresponds to the first principal component (Component 1; 38.3% of the total variance of the data set) and the vertical axis corresponds to the second principal component (Component 2; 14.3% of the total variance of the data set).

The samples of Cluster 2 are located on the middle left part of the graph. The samples of Cluster 1 are located at an intermediate position between the samples of Cluster 2 and Clusters 3 and 4. From left to right along Component 1, TDS increases and groundwater samples evolve gradually from bicarbonate (Clusters 2; Table 2) to brackish (Clusters 1, 3 and 4; Table 2) types. Component 1 is thus defined as representing an increasing salinity gradient from left to right on Fig. 5A.

Chemical element loadings are presented in Table 3. Table 3 reveals that Component 1 loadings are dominated by Cl^- (0.947) and that positive and negative loadings for Component 2 constrain chemical elements in two distinct groups: Group 1 (positive load): Ca^{2+}, Ba^{2+}, Sr^{2+}, and Mn^{2+} and Group 2 (negative load): Mg^{2+}, Na^+, B^{3+}, SiO_2, K^+, $SO_4{}^{2-}$, and $HCO_3{}^-$. Chemical element loadings for Components 1 and 2 are plotted in the correspondence circle in Fig. 5B. The distribution for Group 1 fits with the distribution of samples for Cluster 3, and the distribution for Group 2 fits with the distribution of samples for Cluster 4. Clusters 3 samples and one sample for Cluster 4 are in the upper right quadrant of the correspondence circle. This distribution is due to

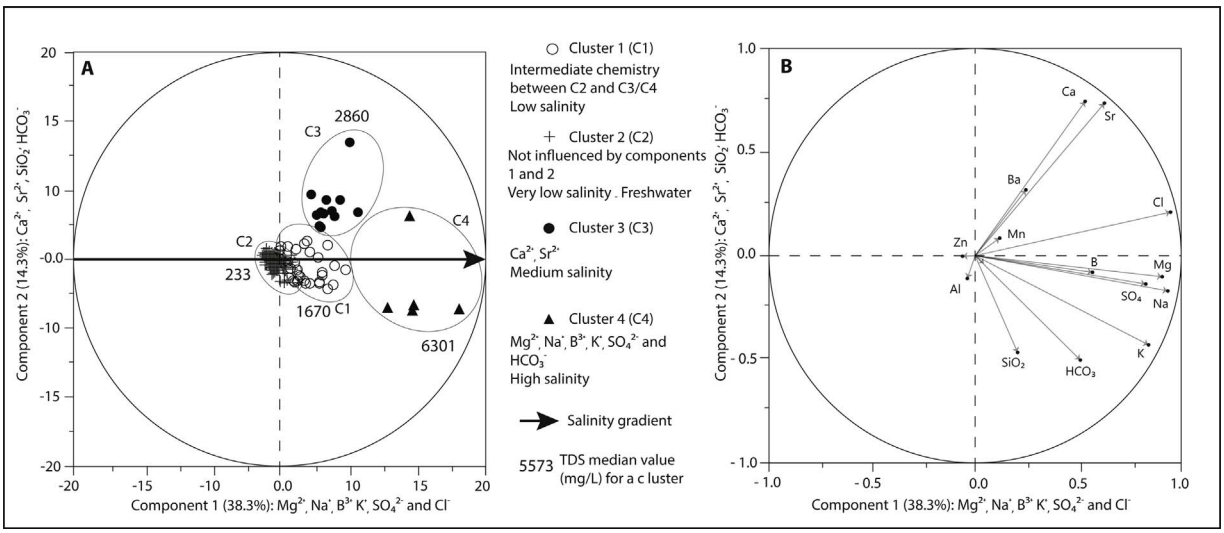

Fig. 5. Graphical presentation of the first two components derived from principal component analysis (PCA). Component 1(K^+, Na^+, Mg^{2+}, $SO_4{}^{2-}$ and Cl^-) explained 38.3% of the total variance of the data set while Component 2 and the vertical axis corresponds to the second principal component (Sr^{2+}, Ca^{2+}) explained 14.3%. A, PCA diagram of samples classified by cluster membership. B, PCA presenting the chemical element loadings.

Table 3
Chemical element loadings for Components 1 and 2 and the explained variance as obtained by principal component analysis (PCA).

Parameter	Component 1	Component 2
K^+	0.839	−0.434
$Na^{+}\cdot$	0.933	−0.172
Ca^{2+}	0.533	0.742
Mg^{2+}	0.909	−0.107
Mn^{2+}	0.121	0.081
B^{3+}	0.561	−0.087
Zn^{2+}	−0.063	−0.008
Cl^-	0.947	0.206
Sr^{2+}	0.626	0.733
SO_4^{2-}	0.830	−0.138
Ba^{2+}	0.248	0.313
Al2+	−0.041	−0.112
SiO_2	0.207	−0.486
HCO_3^-	0.505	−0.506
Explained variance	7.155	0.024
Explained variance (%)	38.3	14.3
Cumulative% of variance	38.3	52.6

Component 2 scores that are positive for Cluster 3 samples and negative for Cluster 4 samples. Cluster 3 correspond exclusively to brackish groundwater collected in the bedrock aquifers (Table 2), their distribution in Fig. 5A suggests that chemical elements in Group 1 (Ca^{2+}, Ba^{2+}, Sr^{2+}, and Mn^{2+}) characterize samples in Cluster 3 and that chemical elements in Group 2 (Mg^{2+}, Na^+, B^{3+}, SiO_2, K^+, SO_4^{2-}, and HCO_3^-) preferentially characterize samples in Cluster 4. Moreover, it also suggests that an increase of the salinity enhances the fingerprint of the rock type aquifer on the groundwater chemistry.

4.3. Geographical distribution of clusters

Fig. 6 presents the geographical distribution of clusters according to the principal rock type units (anorthosite complex, limestones, granite and gneiss). The samples from Cluster 1 are predominately distributed near limestone units (24/30 samples) and a pair

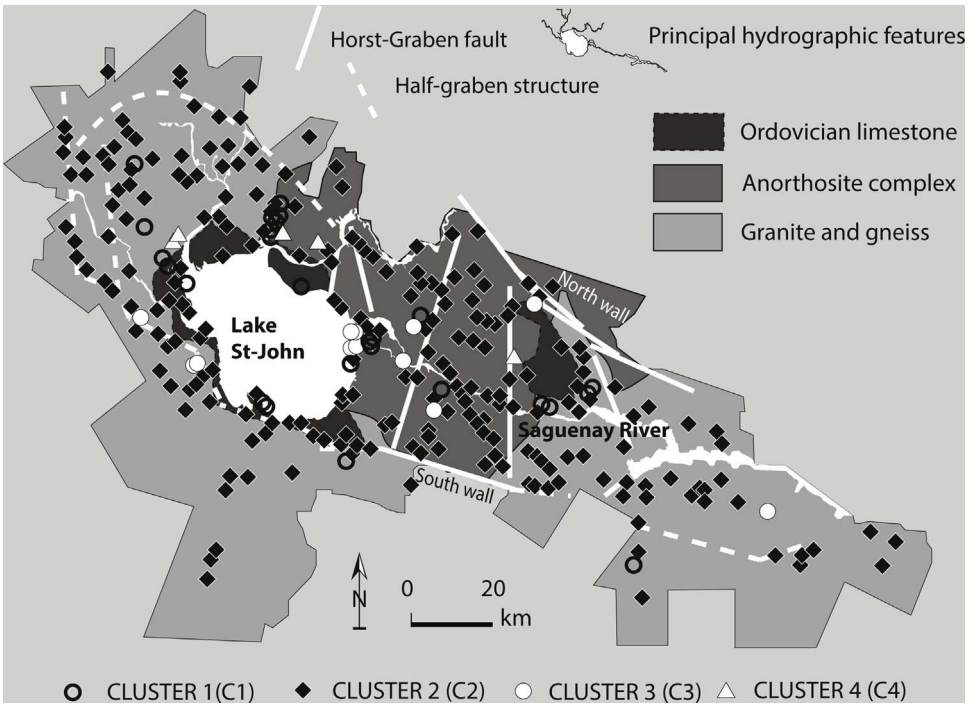

Fig. 6. The simplified geological map of the study area used to locate the 321 groundwater samples according to their belonging cluster. The distribution of Cluster 2 samples is uniform over the region. The samples from Cluster 1 are predominately distributed near limestone units. The Cluster 3 samples are located close to the major geological structures of the graben (fault) and 8 of 12 Cluster 3 samples are located within the anorthosite complex. The samples of Cluster 4 are located around the Lake St. John area.

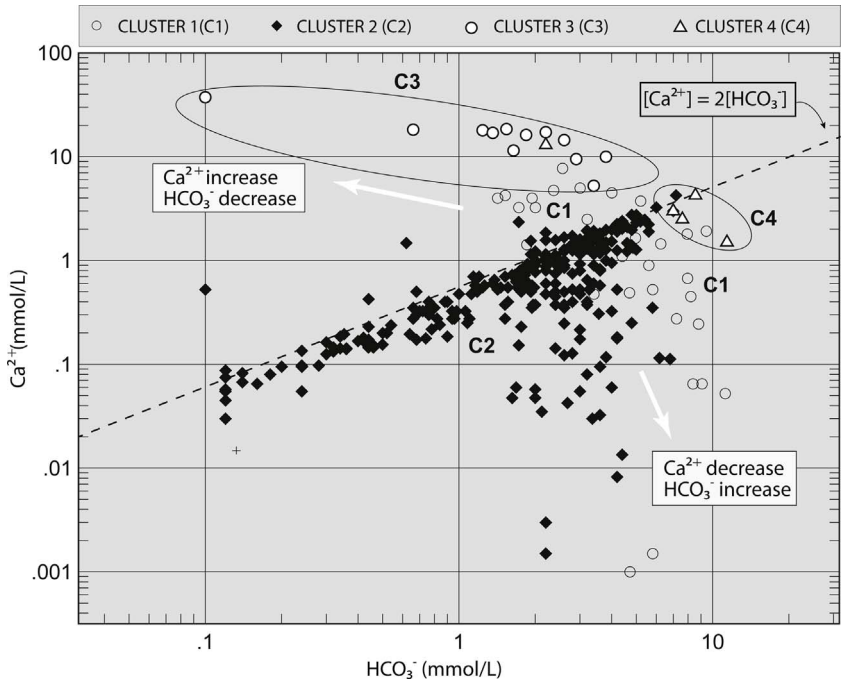

Fig. 7. Log-log plot of bicarbonate versus calcium concentrations (in mmol/L) plotted against to the dissolution trends of calcite ($[Ca^{2+}] = 2[HCO_3^-]$).

of Cluster 1 samples are in the highlands. The distribution of Cluster 2 samples is uniform over the region. The Cluster 3 samples are located close to the major geological structures of the graben (fault) and 8 of 12 Cluster 3 samples are located within the anorthosite complex. The samples of Cluster 4 are near limestone and 4 of 5 of them are located around the Lake St. John area.

5. Discussion

In the following graphs, the samples are represented with respect to their membership in an HCA cluster. Seawater dilution lines were defined using seawater ratios from Goldberg et al. (1971).

5.1. RECHARGE GROUNDWATER AND WATER/ROCK INTERACTIONS − Ca^{2+} vs HCO_3^-

The log–log plot of Ca^{2+} *vs.* HCO_3^- (Fig. 7) indicates the strong positive linear correlation between Ca^{2+} and HCO_3^-, particularly for samples in which the Ca^{2+} concentrations remain unchanged with increasing Cl^- concentrations. The correlation between the Ca^{2+} and HCO_3^- concentrations in Fig. 7 follows the calcite and plagioclase dissolution/precipitation trends (Fig. 7; $[Ca^{2+}] = 2[HCO_3^-]$):

$$3H_2O + 2CO_2 + \underset{\text{(Anorthite)}}{CaAl_2Si_2O_8} \Leftrightarrow \underset{\text{Kaolinite}}{Al_2Si_2O_5(OH)_4} + Ca^{2+} + 2HCO_3^- \quad (1)$$

$$\underset{\text{(Calcite)}}{CaCo_3} + H_2O + CO_2 \Leftrightarrow Ca^{2+} + 2HCO_3^- \quad (2)$$

This observation strengthens the hypothesis that most of the samples of Cluster 2 correspond principally to recharge groundwater, primarily in unconfined hydrogeological environments (Table 2). This observation also implies that the dissolution of calcite and/or anorthite minerals is a fundamental process for inducing the initial geochemical footprint at the beginning of the chemical evolution of groundwater, i.e., in recharge areas.

Another set of reactions leading to the same conclusion is the dissolution of labradorite, a common mineral of the anorthosite complex of the region:

$$\underset{\text{(Labradorite)}}{2NaCaAl_3Si_5O_{16}} + 9H_2O + 6CO_2 \Leftrightarrow 3\ \underset{\text{(Kaolinite)}}{Al_2Si_2O_5(OH)_4} + 4\ SiO_2aq + 2\ Na^+ + 2\ Ca^{2+} + 6HCO_3^- \quad (3)$$

$$\underset{\text{(Labradorite)}}{2NaCaAl_3Si_5O_{16}} + 6H_2O + 6CO_2 \Leftrightarrow \underset{\text{(Kaolinite)}}{2Al_2Si_2O_2(OH)_4} + \underset{\text{(Albite)}}{2NaAlSi_3O_8} + 2Ca^{2+} + 4HCO_3^- \quad (4)$$

Thus, the weathering of labradorite (anorthosite) produces clay, albite (albitization of labradorite) and a Ca-HCO_3 water.

The samples in Cluster 4 exhibit a slight increase in HCO_3^- content that is accompanied by a decrease in Ca^{2+} content. PCA results confirm the influence of HCO_3^- on the chemistry of Cluster 4 samples (Fig. 5).

Ca^{2+} may result from incongruent reactions of magnesian carbonates and having various relationships with HCO_3^-. Incongruent dolomite and limestone dissolution is caused by the difference in solubility products of the two minerals. When water is saturated for calcite, it remains undersaturated for dolomite (or any magnesian limestone) and dissolution of the magnesian minerals will continue and resulting in the precipitation of Ca^{2+} and CO_3^{2-} ions to conserve the equilibrium for calcite (Wigley, 1973; Aquilina et al., 2003). However, these reactions are mostly observed in karst systems (Aquilina et al., 2003) and karst systems are sparse in the study area.

According to Eq. (4), the HCO_3^- content is attributable to the dissociation of water molecules in the presence of CO_2:

$$H_2O + CO_2 \Leftrightarrow H_2CO_3^- \Leftrightarrow H^+ + HCO_3^- \quad (5)$$

The excess of HCO_3^- in Cluster 4 samples relative to the dissolution of calcite/anorthite can be interpreted as the result of any reaction that produces CO_2 (organic matter degradation, sulfate reduction/calcite-dolomite dissolution, etc.). Adding HCO_3^- results in calcite precipitation—according to Eq. (3) in reverse—and thus the removal of dissolved Ca^{2+} from the solution and a decrease in the Ca^{2+} concentration.

The diminishing HCO_3^- concentrations in the Cluster 3 samples is accompanied by an increase in Ca^{2+} content (Fig. 7). This agrees with the PCA results that showed the predominant role of Ca^{2+} in the chemistry of the samples of Cluster 3 (Table 2 and Fig. 5). When groundwater reaches calcite saturation in the presence of CO_2, Ca^{2+} precipitates as secondary calcite (Eq. (5); Stober and Bucher, 1999a,b). This process is evident in the minerals observed in the fractures, veins and cavities of the Canadian Shield rocks (Gascoyne and Kamineni, 1994). With the consumption of all available CO_2, no more HCO_3^- is available in solution. However, Ca^{2+} will continue to be released during anorthite plagioclase alteration according to Eq. (6) (Stober and Bucher, 1999a,b), in which the CO_2 in Eq. (1) is replaced by H^+ ions.

$$\underset{\text{(Anorthite)}}{CaAl_2Si_2O_8} + 2H_2O + CO_2 \rightarrow \underset{\text{(Kaolinite)}}{Al_2Si_2O_5(OH)_4} + \underset{\text{(Calcite)}}{CaCO_3} \quad (6)$$

$$\underset{\text{(Anorthite)}}{CaAl_2Si_2O_8} + 2H^+ + H_2O \rightarrow Ca^{2+} + \underset{\text{(Kaolinite)}}{Al_2Si_2O_5(OH)_4} \quad (7)$$

The control of the plagioclase weathering process on the chemical evolution of groundwater within fractured rock aquifers is also suggested by the PCA results. Ba^{2+} and Sr^{2+} are commonly incorporated as trace elements in the crystalline structure of feldspar plagioclase minerals (Beaucaire and Michard, 1982; Hem, 1985). In Fig. 5, these two chemical elements, in particular, characterize the chemistry Cluster 3 samples.

5.2. Salinization processes

The Cl^-/Br^- ratios (based on ppm) are often used to provide insight into the marine origin of salinity in groundwater (Carpenter, 1978; Frape et al., 1984; Montcoudiol et al., 2014). In comparing ratios with seawater ratios ($Cl^-/Br^- = 288$; Stober and Bucher, 1999a,b), groundwater Cl^-/Br^- ratios can indicate if a brine has undergone Br^- enrichment or Cl^- depletion (relative to seawater). For comparison, water derived from dissolved Tertiary halite deposits of the East African Rift System (EARS) has a Cl^-/Br^- ratio of 2400 while the average Cl^-/Br^- ratio for crystalline rocks is below $Cl^-/Br^- = 100$ (Stober and Bucher, 1999a,b).

In Fig. 8C, Br^- enrichment (or Cl^- depletion) relative to seawater is apparent for Cluster 3 samples, whereas the samples of Cluster 4 tend to follow the seawater dilution line. Cluster 4 waters have a Cl^-/Br^- ratio = 266 (Cl^-/Br^- seawater = 283; Goldberg et al., 1971). Cluster 3 waters have a Cl^-/Br^- ratio around 88, close to that of crystalline rocks (Stober and Bucher, 1999a,b) suggesting a basement origin for chloride in Cluster 3. Many Cluster 2 samples also have low Cl^-/Br^- ratios (~85) suggesting that salinization is related to basement fluids for these samples as well.

The Na^+/Cl^- ratios for Cluster 3 are slightly depleted in Na^+ relative to those of seawater (Fig. 8A). Na^+/Cl^- ratios lower than those in seawater have been observed in saline groundwater in granitic rocks in the United Kingdom (Edmunds et al., 1984) and France (Beaucaire et al., 1999). In both studies, the low Na^+/Cl^- ratios relative to seawater are attributed to equilibration with secondary aluminosilicates and thus a predominance of water/rock interaction processes. Cluster 3 samples follow this trend. The Na^+/Cl^- ratios for Cluster 4 samples are slightly enriched in Na^+ and are very similar to the Na^+/Cl^- ratios of seawater.

Enrichment relative to seawater was also observed for the Ca^{2+}/Cl^- ratios (Fig. 8B), particularly for the Cluster 3 samples relative to the Cluster 4 samples. In this figure, the linear relationship between Ca^{2+} and Cl^- is striking. Calcium exhibits a strong positive linear correlation with Cl^- in deep saline groundwaters in the Canadian Shield (Frape et al., 1984; Frape and Fritz, 1987; Bottomley, 1996).The Ca^{2+}/Na^+ ratios for the Cluster 4 samples are very similar to those of seawater (Fig. 9). The Cluster 4 samples tend to reach the seawater dilution line (Fig. 9). For these samples, the salinization process might then correspond to the mixing between a seawater end-member (Na-Cl of Cluster 4) and more diluted water containing (Ca, Na)-HCO_3 (Clusters 1 and 2) (Salinization path 2; Fig. 9).

Gascoyne and Kamineni (1994) presented a model for different types of crystalline rocks in the Canadian Shield, in which the near surface groundwater (Ca-HCO_3 in composition) evolves into slightly more mature groundwater (Na-HCO_3 in composition) as it moves along the flow paths and increases with depth (~250 m). At greater depths (> 1000 m), all groundwaters tend toward a (Ca-Na)-Cl composition. For samples of Cluster 3, the salinization process corresponds to the geochemical evolution from Cluster 2 (Ca-HCO_3) to Cluster 3 (Ca-(Na)-Cl) groundwater (Salinization path 1; Fig. 9).

Cluster 1 samples stand in an intermediate position between both Clusters 2 and 3 and between Clusters 2 and 4 (Fig. 9). Cluster 1 as well as some Cluster 2 samples within the field of Cluster 1 samples correspond to groundwater that may have undergone mixing

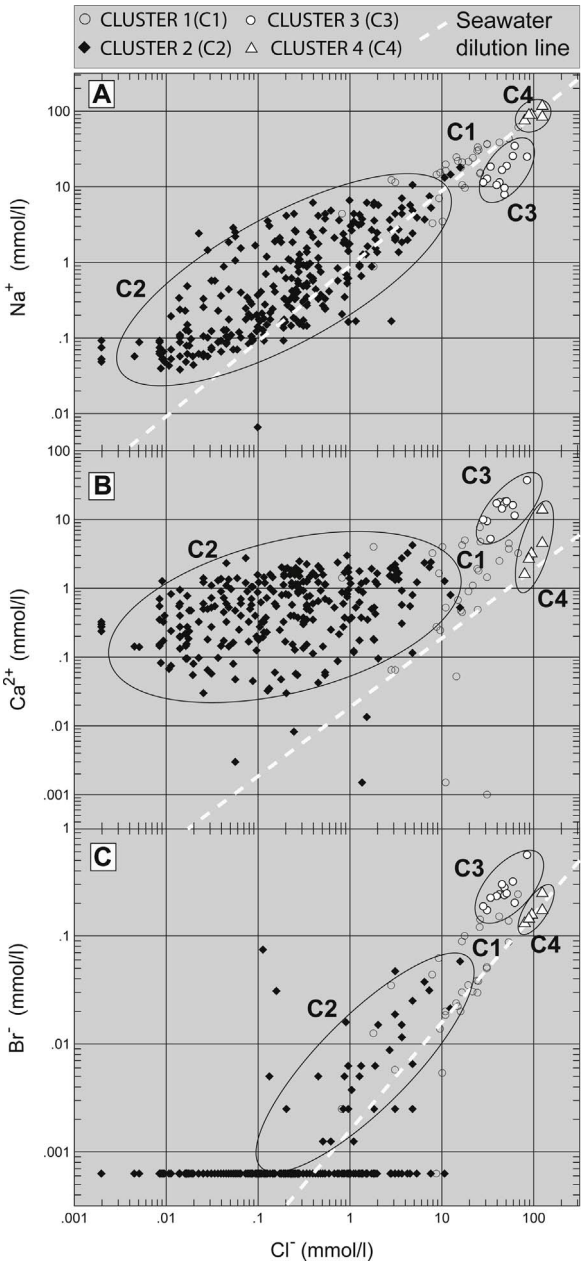

Fig. 8. Log-log plots of A, Na^+ versus Cl^- concentrations (in mg/L) and B, Ca^{2+} versus Cl^- concentrations (in mg/L); and C: Br^- versus Cl^- concentrations (in mg/L). Seawater (SW) dilution lines were defined using seawater ratios from Goldberg et al. (1971).

and dilution between fresh and brackish groundwater that evolved along Salinization paths 1 or 2.

5.3. Ca^{2+}_{WATER}-$Na^{+}_{MINERAL}$ ION exchange

Ion exchange reactions in these confining layers may underlie the desorption of Na^+ from the Na-Cl-rich seawater according to Eq (8) (where $X_{(s)}$ represents the solid matter of the confining layer, which plays the role of cation exchanger):

$$Ca^{2+} + 2Na\text{-}X_{(s)} \Leftrightarrow 2Na^{+} + Ca\text{-}X_{(s)} \quad (8)$$

When freshwater (Ca-HCO_3 in composition) infiltrates and circulates in confined granular deposits and contacts the confining layers, Ca^{2+} is taken up from the freshwater to replace Na^+, which is released from the cation exchanger in the groundwater (Eq. (8)).

This process is known to occur in coastal aquifers (Appelo and Postma, 2005) and has been observed within the Basses-

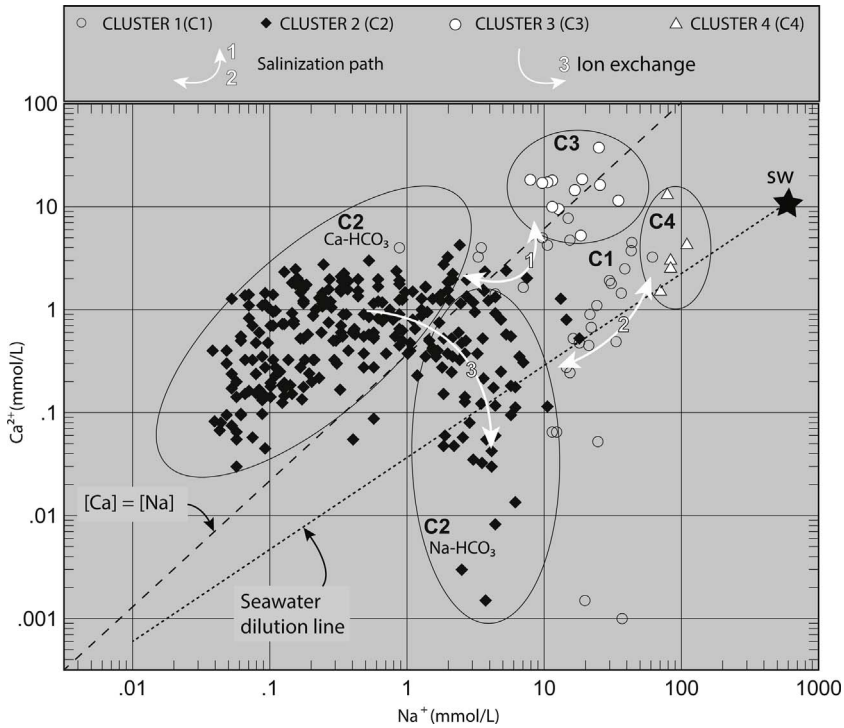

Fig. 9. Log-log plots of Na^+ versus Ca^{2+} concentrations (in mmol/L). The seawater (SW) dilution line was defined using the seawater ratios from Goldberg et al. (1971). Salinization path 1 corresponds to the geochemical evolution from Cluster 2 (Ca-HCO_3) to Cluster 3 (Ca-(Na)-Cl) groundwater samples. Salinization path 2 corresponds to the mixing between a seawater end-member (Na-Cl of Cluster 4) and more diluted water containing (Ca, Na)-HCO_3 (Cluster 2). Salinization path 3 corresponds to groundwater evolution under Ca^{2+}_{WATER}-$Na^{+}_{MINERAL}$ ion exchange process.

Laurentides aquifer. In the Basses-Laurentides aquifer system, granular aquifers are confined by marine Pleistocene clays deposited during the Champlain Sea episode (Cloutier et al., 2010). In this case, clays play the role of cation exchanger liberating Na^+ in groundwater.

Samples in Cluster 4 are all Na-Cl type reflecting a marine origin. Cluster 4 samples are the closest samples to the seawater end-member in Fig. 9 and most Cluster 4 samples plot near the seawater dilution line. Some of the samples for Cluster 1 plot in an intermediate position between Na-HCO_3 samples in Clusters 2 and 4 and are aligned along the seawater dilution line. Path 2 in Fig. 9 corresponds to the salinization process that brings Na-HCO_3 groundwater to a Na-Cl water type. Cluster 4 then represents an end-member of the mixing trend between a seawater end-member and the more diluted water that prevails in confined aquifers within the study area.

The combination of reactions 3 and 4 for the plagioclase dissolution shows that $2\,Na^+ = Ca^{2+}$. A gradually changing Na^+/Ca^{2+} ratio of the groundwater may then be related to the dissolution/precipitation kinetics of feldspars. In Fig. 9, samples that follow Salinization path 3 correspond to groundwater evolving from a Ca-HCO_3 facies to a Na-HCO_3 facies according to this kinetic process.

5.4. Microcline weathering

Mineralogical analyses performed on deep marine deposits in some areas of the SLSJ region showed that microcline and illite represent 41% and 21% of the argillaceous fraction of clay, respectively (Gravel; 1974). K-feldspar (microcline) transformation into the clay mineral (illite), is represented by:

$$3\ \underset{\text{(Microcline)}}{KAlSi_3O_8} + 2H^+ \rightarrow 2\,K^+ + 6SiO_2 + \underset{\text{(Illite)}}{KAl_3Si_3O_{10}(OH)_2} \quad (9)$$

According to the PCA results (Fig. 5), SiO_2 and K^+ are related to samples in Cluster 4. The influence of SiO_2 and K^+ on the chemistry of Cluster 4 results from the chemical breakdown of microcline and it confirms that the weathering of silicate minerals occurs more efficiently within the regional aquitard than in the bedrock.

5.5. General geochemical evolution path in the slsj aquifer systems

The combination of HCA, PCA and binary graphs demonstrates that the occurrence of two distinct salinization paths depends on the hydrogeological context. Based on the content of major elements, the general geochemical evolution paths of groundwater within the SLSJ aquifer systems are presented in the Piper diagram in Fig. 10. The samples are presented according to the HCA cluster to

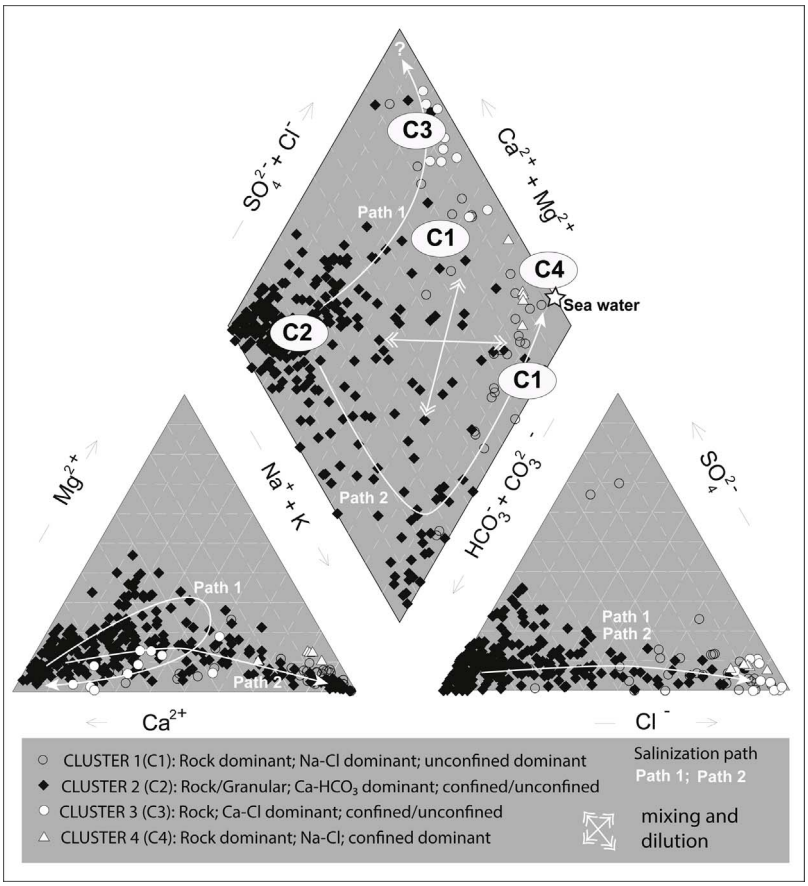

Fig. 10. Piper diagram of the general evolution pathways of groundwater within the Saguenay-Lac-Saint-Jean aquifer systems. Mixing and dilution occur at different rates during the evolution of groundwater having different origins (mixing and dilution zones). From the recharge area, the evolution of groundwater follows two possible paths. The first (Path 1) occurs as groundwater flows through crystalline bedrock aquifers, which induces a change in the anion composition from HCO_3^- -dominant (Cluster 2) to Cl^- -dominant (Cluster 3). In this path, groundwater evolves by water/rock interactions toward a Ca-Cl end-member. The second path begins with the weathering of feldspath and results in the movement of the samples from Ca-HCO_3 to Na-HCO_3. Ca^{2+}_{water}-Na^+ mineral ion exchange, solute diffusion from the Laflamme Sea clay aquitard and/or mixing with Laflamme seawater provoke the evolution of recharge Ca-HCO_3 groundwater (Cluster 2) to Na-HCO_3 groundwater and brackish groundwater (Na-Cl in composition, Cluster 4).

which they belong.

Cluster 2 samples (Ca,Na-HCO3) reflect the first stage of groundwater evolution as the cation composition changes from Ca^{2+} dominant to Na^+ dominant, which is explained by ion exchange processes in the presence of the marine clay aquitard and further explained by the feldspar dissolution/precipitation kinetics in the bedrock. Then, the evolution of groundwater follows two possible paths.

The first path occurs as groundwater flows through the crystalline bedrock aquifers, which induces a change in the anion composition from HCO_3^- -dominant (Clusters 2) to Cl^- -dominant end-members (Clusters 3 and 4). According to the first path (Path 1), groundwater tends to evolve by water/rock interactions toward a Ca-Cl end-member. This evolution is accompanied by the simultaneous increase of the Ca^{2+}, Sr^{2+} and Ba^{2+} contents of groundwater. The second path begins with Ca^{2+}_{water}-Na^+mineral ion exchange and results in the transformation of the samples from Ca-HCO_3 to Na-HCO_3 (Fig. 10; Path 2). Path 2 represents the evolution of groundwater due to a salinization path within the confined aquifers that are in contact with the regional aquitard and possible groundwater mixing with the Pleistocene Laflamme Sea end-member. The seawater could be trapped in the regional aquitard (solute diffusion) or may be stagnant (mixing) in some part of the aquifer (Cloutier et al., 2010). This latter combination of processes (cation exchange and/or leaching of saltwater trapped in the regional aquitard) is grouped in this study under the term “water/clay interactions”. Ion exchange, solute diffusion from the Laflamme Sea clay aquitard and/or mixing with Laflamme seawater cause the evolution of Cluster 2 (recharge Ca-HCO_3 groundwater to Na-HCO_3 groundwater) to Cluster 4 (brackish groundwater Na-Cl in composition). Following this latter trend, the chemistry of the groundwater tends to evolve toward an end-member having a composition that is like that of present seawater, i.e., Na-Cl-rich. According to the PCA, this evolution is accompanied by a simultaneous increase of the Mg^{2+}, SiO_2, K^+ and SO_4^{2-} contents of groundwater.

Fig. 11 is a generalized cross-section showing the different salinization pathways occurring in the SLSJ area. The topography caused by a graben structure ($>$ 1000 m) displays a connection between water composition and groundwater flow driven by the

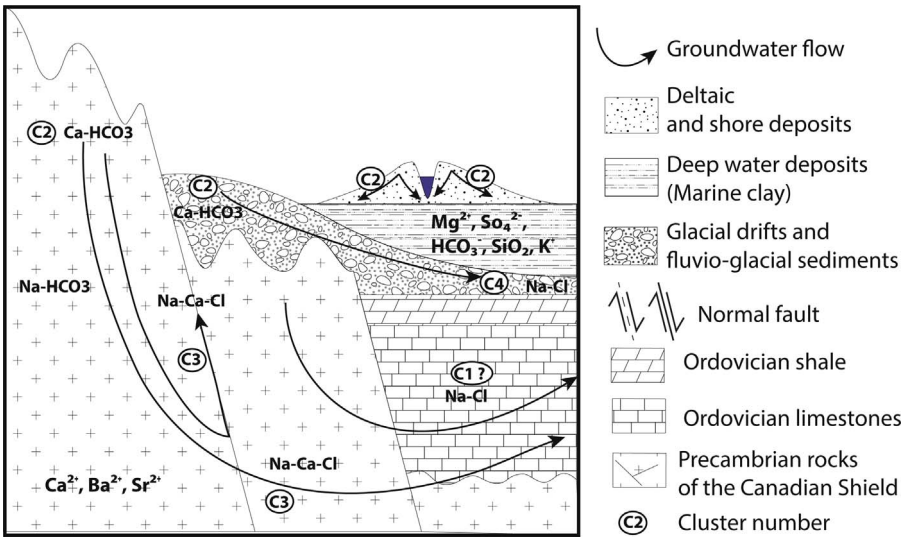

Fig. 11. Generalized cross-section showing the different salinization pathways occurring in the SLSJ area. Bedrock groundwater evolves from Cluster 2 (Ca,Na-HCO_3, unconfined environment) to Cluster 3 (Ca,Na-Cl; rock dominated) by interactions with basement fluids (water-rock interactions) coming up along the graben fault system (groundwater flow line). The distribution of Cluster 1 close by Limestone units (Fig. 6) and the hydrogeological information related to Cluster 1 (Fig. 4: Na-Cl type in confined bedrock aquifers) suggest that Cluster 1 represent a seawater end-member of groundwater evolving in contact with the Ordovician limestone. The groundwater in the granular aquifers exhibits an evolution from the recharge groundwater (Ca-HCO_3) by Ca^{2+}_{water}-$Na^{+}_{mineral}$ ion exchange process in a confined environment (Na-HCO_3; Cluster 2) and possible mixing with the Laflamme seawater end-member (Na-Cl; Cluster 4). This latter evolution might also be observed in bedrock aquifers where confining conditions prevail.

topographic gradient. Bedrock groundwater evolves from Cluster 2 (Ca,Na-HCO_3, unconfined environment) to Cluster 3 (Ca,Na-Cl; rock dominated) by interactions with basement fluids (water-rock interactions, e.g. Cl^-/Br^- mass ratios of 88 derived from Fig. 8) coming up along the graben fault system. The distribution of Cluster 3 samples along major faults in Fig. 6 also suggests the upwelling of basement fluids toward the surface. In the crystalline basement, the dissolution/precipitation kinetics of feldspars induce a gradual changing of the chemical facies from Ca-HCO_3 to Na-HCO_3 (Cluster 2).

Confining conditions dominate Cluster 4 (Fig. 4; Table 2). The groundwater in the granular aquifers exhibits an evolution from the recharge groundwater of Cluster 2 by ion exchange (Cluster 2 Na-HCO_3) in a confined environment and possible mixing with the Laflamme seawater end-member (e.g., Cl^-/Br^- mass ratios of 266 derived from Fig. 8; Cluster 4). This latter evolution might also be observed in bedrock aquifers where confining conditions prevail.

Cluster 1 samples are dominated by Na-Cl waters from confined bedrock aquifers (Fig. 4). The samples from Cluster 1 are predominately distributed near limestone units (24/30 samples) (Fig. 6) and may then represent a seawater end-member of groundwater evolving in contact within the confined Ordovician limestone.

The end-members of the salinization paths, represented by Clusters 3 and 4, are thus identified and can be distinguished based on the relative concentrations of the following trace elements: Ca^{2+}, Sr^{2+}, Ba^{2+} for Cluster 3 and Mg^{2+}, SiO_2, K^+, SO_4^{2-}, and HCO_3^- for Cluster 4 (Fig. 5). Mixing and dilution (Fig. 10) occur at different rates during the evolution of groundwater having different origins in response to the specific hydrogeological context prevailing locally in the region.

6. Summary and conclusions

In this paper, groundwater evolution paths that account for the chemical characteristics of a large dataset obtained from groundwater analyses in a regional-scale study has been described. The dissolution of calcite and/or plagioclase minerals controls the chemical background of recharge groundwater. Anorthite plagioclase weathering is more effective in bedrock aquifers, and the Ca^{2+}_{water}-$Na^{+}_{mineral}$ ion exchange process is dominant in confined aquifers. In addition, there is mixing with a seawater end-member where confining conditions by the regional aquitard are prevailing. In the crystalline bedrock, mixing with deep brackish groundwater by topographically driven groundwater flow appears to be a possibility in the Lake St. John area.

The combination of HCA, PCA and binary graphs identifies two distinct salinization paths occur: 1) an evolution by water/rock interactions; and 2) an evolution from the recharge groundwater by water/clay interactions and groundwater mixing. The first evolution path is specific to fractured rock aquifers. The term water/clay interactions was introduced in this paper to account for a combination of processes, namely: ion exchange and/or leaching of salt water trapped in the regional aquitard. Mixing with fossil seawater present in the aquifer might also increase the groundwater salinity.

Based on the results obtained using PCA, clusters can be distinguished according to the relative concentrations of the following trace elements: Ca^{2+}, Sr^{2+} and Ba^{2+} for Cluster 3 (water/rock interactions) and HCO_3^-, Mg^{2+}, SiO_2, K^+ and SO_4^{2-} for Cluster 4 (water/clay interactions). One of the main processes controlling the groundwater chemistry in confined aquifers is believed to be the degradation of organic matter and/or any other reaction that produces CO_2. Another process could be the silicate alteration process,

more specifically microcline plagioclase weathering.

The percentage of cumulative variance obtained via PC 1 and 2 is 52.6%. This suggests that 50% of the variance of the dataset cannot be explained by the first two components (salinity). Other components need to be investigated to establish a more global portrait of regional hydrogeochemistry. Further work should also focus on identifying reliable tracers of the two salinization paths using Factorial Analysis (FA). In contrast to PCA, the emphasis of FA is explaining covariances instead of the total variance of a dataset. Thus, FA could be used to highlight highly correlated chemical parameters within the dataset and shed new light on the chemical nature of the samples.

Next steps should prioritize an improved knowledge of the different rock types and their geochemical properties. Compilation of the existing geochemical data on rocks and sediments should be coupled with the sampling of outcrops to investigate the mineralogical assemblages of the various regional rocks (via thin section analysis). Leaching experiments should also be performed to obtain different specific ionic ratios, as for instance the Cl^-/Br^- ratio. Finally, a new sampling campaign focused on isotopic data (^{18}O, ^{2}H, ^{13}C, etc.) and residence time constraints could contribute to deciphering the data set, especially the origins of the saline end-members.

This study—derived from a routine chemical analysis of water quality—provides a new understanding of the chemical evolution of groundwater that is of interest in conceptualizing the dynamics of groundwater, such as flow patterns and hydraulic connectivity between aquifers. With a better understanding of the chemical characteristics of the salinization paths, the major, minor and trace element chemistry of groundwater becomes a relevant tool for investigating groundwater dynamics, such as the interconnectivity of aquifer systems or groundwater flow dynamics according to gravity-driven flow processes. With a better knowledge of the geochemistry of the porous and the fractured matrix of regional aquifers, as well as of the geochemistry of aquitards present in the SLSJ region, this study may leads to discussions on the spatial and temporal evolution of groundwater quality with respect to the prevailing geochemical paths (water/rock and/or water/clay interactions).

Acknowledgements

This project was funded by the Natural Sciences and Engineering Research Council of Canada (NSERC), theFonds de recherche du Québec − Nature et technologies (FRQNT), the Fondation de l'université du Québec à Chicoutimi (FUQAC), Rio Tinto Alcan (RTA), and the Programme d'acquisition de connaissances sur les eaux souterraines of Quebec (PACES), with contributions from the Quebec Ministère du Développement durable, de l'Environnement, de la Faune et des Parcs (MDDEFP), and the five county municipalities of the SLSJ region (Domaine-du-Roy, Du-Fjord-Du-Saguenay, Lac-Saint-Jean-Est; Maria-Chapdelaine and the City of Saguenay). The authors wish to acknowledge Dr. Ingrid Stober and the anonymous reviewers for their meaningful input, Professor Philippe Page from the University du Quebec à Chicoutimi (UQAC) who gave us the benefit of his extensive experience in geochemistry, technician David Noël for his multiple skills in field hydrogeology, all the students involved in the project as field assistants and, finally, the research assistants M. Lambert, A. Moisan, M.L. Tremblay and D. Germaneau for their help with the PACES project. In addition, the authors wish to thank the well owners who graciously provided access to their groundwater intakes for sampling.

Appendix A. Supplementary data

Supplementary data associated with this article can be found, in the online version, at http://dx.doi.org/10.1016/j.ejrh.2017.07.004.

References

Alvin, C.R., 2002. Methods of Multivariate Analysis. Wiley Interscience.
Appelo, C.A.J., Postma, D., 2005. Geochemistry, Groundwater Pollution. A Balkema Publishers, Amsterdam.
Aquilina, L., Ladouche, B., Doerfliger, N., Bakalowicz, M., 2003. Deep water circulation, residence time, and chemistry in a karst complex. Ground Water 41 (6), 790–805.
Aquilina, L., et al., 2015. Impact of climate changes during the last 5 million years on groundwater in basement aquifers. Sci. Rep. 5.
ArandaCirerol, N., Herrera-Silveira, J.A., Comín, F.A., 2006. Nutrient water quality in a tropical coastal zone with groundwater discharge northwest Yucatan, Mexico. Estuar Coast. Shelf Sci. 68, 445–454.
Beaucaire, C., Michard, G., 1982. Origin of dissolved minor elements (Li, Rb, Sr, Ba) in superficial waters in a granitic area. Appl. Geochem. 16, 247–258.
Beaucaire, C., Gassama, N., Tresonne, N., Louvat, D., 1999. Saline groundwaters in the hercynian granites (Chardon Mine, France): geochemical evidence for the salinity origin. Appl. Geochem. 14, 67–84.
Bottomley, D.J., et al., 1999. The origin and evolution of Canadian Shield brines: evaporation or freezing of seawater? New lithium isotope and geochemical evidence from the Slave craton. Chem. Geol. 155, 295–320.
Bottomley, D.J., Conrad Gregoire, D., Raven, K.G., 1994. Saline ground waters and brines in the Canadian Shield: geochemical and isotopic evidence for a residual evaporite brine component. Geochim. Cosmochim. Acta 58, 1483–1498.
Bouchard, R., Dion, D.J., Tavenas, F., 1983. Origine de la préconsolidation des argiles du Saguenay, Qc. Can. Geotech. J. 20, 315–328.
Box, G.E., Cox, D.R., 1964. An analysis of transformations. J. Royal Stat. Soc. Ser. B (Methodological) 211–252.
Brown, C.E., 1998. Applied Multivariate Statistics in Geohydrology and Related Sciences. Springer, Berlin.
Bucher, K., Stober, I., 2010. Fluids in the upper continental crust. Geofluids 10, 241–253.
Bucher, K., Stober, I., Seelig, U., 2012. Water deep inside the mountains: unique water samples from the Gotthard rail base tunnel. Switzerland Chem. Geol. 334, 240–253.
CERM-PACES, 2013. Résultats du programme d'acquisition de connaissances sur les eaux souterraines du Saguenay-Lac-Saint-Jean, Centre d'étude sur les ressources Minérales de l'Université du Québecà Chicoutimi.
Carpenter, A.B., 1978. Origin and chemical evolution of brines in sedimentary basins, SPE Annual Fall Technical Conference and Exhibition. Soc. Pet. Eng.
Chebotarev, I.I., 1955. Metamorphism of natural waters in the crust of weathering 1-2-3. Geochim. Cosmochim. Acta 8, 22–48.

Chesnaux, R., Rafini, S., Elliott, A.-P., 2012. A numerical investigation to illustrate the consequences of hydraulic connections between granular and fractured-rock aquifers. Hydrogeol. J. 20, 1669–1680.
Cloutier, V., Lefebvre, R., Savard, M.M., Bourque, É., Therrien, R., 2006. Hydrogeochemistry and groundwater origin of the Basses-Laurentides sedimentary rock aquifer system, St. Lawrence Lowlands, Quebec, Canada. Hydrogeol. J. 14, 573–590.
Cloutier, V., Lefebvre, R., Therrien, R., Savard, M.M., 2008. Multivariate statistical analysis of geochemical data as indicative of the hydrogeochemical evolution of groundwater in a sedimentary rock aquifer system. J. Hydrol. 353, 294–313.
Cloutier, V., Lefebvre, R., Savard, M.M., Therrien, R., 2010. Desalination of a sedimentary rock aquifer system invaded by Pleistocene Champlain Seawater and processes controlling groundwater geochemistry. Environ. Earth Sci. 59, 977–994.
Daigneault, R., et al., 2011. Rapport Final Sur Les Travaux De Cartographie Des Formations Superficielles réalisés Dans Le Territoire Municipalisé Du Saguenay-Lac-Saint-Jean (Québec) Entre 2009 Et 2011 Govern. Report MRNF (Qc).
Davis, J., 2002. Statistics and Data Analysis in Geology. John Wiley & Sons, New York.
Desbiens, S., Lespérance, P.J., 1989. Stratigraphy of the ordovician of the lac saint-Jean and Chicoutimi outliers quebec, can. J. Earth Sci. 26, 1185–1202.
Dessureault, R., 1975. Hydrogéologie Du Lac Saint-Jean, Partie Nord-est. Québec: MRN, Dir. Gen. Eaux, Service Des Eaux Souterraines.
Dionne, J., Laverdière, C., 1969. Sites fossilifères du golfe de Laflamme. Rev. Géogr. Montréal 23, 259–270.
Douglas, M., Clark, I., Raven, K., Bottomley, D., 2000. Groundwater mixing dynamics at a Canadian Shield mine. J. Hydrol. 235 (1), 88–103.
Du Berger, R., et al., 1991. The Saguenay (Quebec) earthquake of November 25, 1988: seismologic data and geologic setting. Tectonophysics 186, 59–74.
Edmunds, W.M., Andrews, J.N., Burgess, W.G., Kay, R.L.F., Lee, D.J., 1984.. The evolution of saline and thermal groundwaters in the Carnmenellis granite. Mineral. Mag. 48, 407–424.
Edmunds, W., Kay, R., McCartney, R., 1985. Origin of saline groundwaters in the Carnmenellis granite (Cornwall, England): natural processes and reaction during hot dry rock reservoir circulation. Chem. Geol. 49, 287–301.
Farnham, I.M., Singh, A.K., Stetzenbach, K.J., Johannesson, K.H., 2002. Treatment of nondetects in multivariate analysis of groundwater geochemistry data. Chemometr Intell. Lab. Syst. 60 (1), 265–281.
Frape, S., Fritz, P., 1987. Geochemical trends for groundwaters from the Canadian Shield: saline water and gases in crystalline rocks. Geol. Assoc. Can. 33, 19–38.
Frape, S.K., Fritz, P., McNutt, R.H.t., 1984. Water-rock interaction and chemistry of groundwaters from the Canadian Shield. Geochim. Cosmochim. Acta 48, 1617–1627.
Frape, S., Blyth, A., Blomqvist, R., McNutt, R., Gascoyne, M., 2003. Deep fluids in the continents: II: Crystalline rocks. Treatise Geochem. 5, 541–580.
Fritz, P., Frape, S.K., 1982. Saline groundwaters in the canadian shield – a first overview. Chem. Geol. 36, 179–190.
Fritz, P., Frape, S.K., Drimmie, R.J., Appleyard, E.C., Hattori, K., 1994. Sulfate in brines in the crystalline rocks of the Canadian shield. Geochim. Cosmochim. Acta 58, 57–65.
Fyfe, W.S., Price, N.J., Thompson, A.B., 1978. Fluids in the Earth's Crust. Elsevier, Amsterdam, pp. 383.
Güler, C., Thyne, G.D., McCray, J.E., Turner, K.A., 2002. Evaluation of graphical and multivariate statistical methods for classification of water chemistry data. Hydrogeol. J. 10, 455–474.
Gascoyne, M., Kamineni, D.C., 1994. The hydrogeochemistry of fractured plutonic rocks in the Canadian Shield. Appl. Hydrogeol. 2, 43–49.
Gascoyne, M., Davison, C.C., Ross, J., Pearson, R., 1987. Saline groundwaters and brines in plutons in the Canadian Shield: saline water and gases in crystalline rocks. Geol. Assoc. Can. 53–68.
Gascoyne, M., Stroes-Gascoyne, S., Sargent, F., 1995. Geochemical influences on the design, construction and operation of a nuclear waste vault. Appl. Geochem. 10, 657–671.
Ghesquière, O., Walter, J., Chesnaux, R., Rouleau, A., 2015. Scenarios of groundwater chemical evolution in a region of the Canadian Shield based on multivariate statistical analysis. J. Hydrol. Reg. Stud. 4, 246–266.
Goldberg, E., Broecker, W., Gross, M., Turekian, K., 1971. Radioactivity in the Marine Environment. National Academy of Science, Washington, DC, pp. 137.
Guha, J., Kanwar, R., 1987. Vug brines-fluid inclusions A key to the understanding of secondary gold enrichment processes, the evolution of deep brines in the Canadian Shield. Saline water and gases in crystalline rocks. Geol. Assoc. Can. Ottawa: Geol. Assoc. Can. Spec. Pap. 33, 95–101.
Hébert, C., Lacoste, P., 1998. Géologie de la région de jonquière-Chicoutimi (SNRC 22D). Qc. MRN Sect. Mines.
Hébert, C., Van Breemen, O., 2004. Mesoproterozoic basement of the Lac St. Jean Anorthosite Suite and younger Grenvillian intrusions in the Saguenay region, Québec: structural relationships and U-Pb geochronology. Geol. Soc. Am. Mem. 197, 65–79.
Health Canada, (2007). Guidelines for Canadian drinking water quality: summary table. Federal–Provincial–Territorial Committee on Drinking Water, July 2015. http://www.hc-sc.gc.ca/ewh-semt/pubs/water-eau/sum_guide-res_recom/index-eng.php.
Hem, J.D., 1985. Study and interpretation of the chemical characteristics of natural water, 2254. Department of the Interior, US Geological Survey.
Hervet, M., Van Breemen, O., Higgins, M., 1994. U–Pb crystallisation ages of intrusive rocks near the southeast margin of the Lac-St-Jean anorthosite complex, Grenville Province, Quebec. R adiogen. Quebec. R adiogen. Age Isot. Stud. Rep. 8, 115–124.
Higgins, M.D., Van Breemen, O., 1996. Three generations of anorthosite-mangerite-charnockite-granite (AMCG) magmatism, contact metamorphism and tectonism in the Saguenay-Lac-Saint-Jean region of the Grenville Province, Canada. Precamb. Res. 79, 327–346.
Hounslow, A., 1995. Water Quality Data: Analysis and Interpretation. CRC press.
Kamineni, D.C., 1987. Halogen-bearing minerals in plutonic rocks: a possible source of chlorine in saline groundwater in the Canadian Shield. Saline water and gases in crystalline rocks. Geol. Assoc. Can. Spec. Pap. 33, 69–79.
Kharaka, Y., Hanor, J., 2003. Deep fluids in the continents: i: sedimentary basins. Treatise Geochem. 5, 499–540.
LaSalle, P., Tremblay, G., 1978. Dépôts Meubles: Saguenay Lac Saint-Jean. (MRN Dir. gén).
Lahermo, P., Lampen, P., 1987. Brackish and saline groundwaters in Finland: saline water and gases in crystalline rocks. Geol. Assoc. Can. Spec. Pap. 33, 103–109.
Laurin, A.F., Sharma, K.N.M., 1975. Région Des Rivières Mistassini, Péribonca, Saguenay: Mistassini, Péribonca, Saguenay Rivers Area: Grenville. pp. 1965–1967 (MRN Dir. gén).
Lemieux, J.M., Sudicky, E., Peltier, W., Tarasov, L., 2008. Dynamics of groundwater recharge and seepage over the Canadian landscape during the Wisconsinian glaciation. J. Geophys. ResEarth Surf. 113, F1.
Lodemann, M., Fritz, P., Wolf, M., Ivanovich, M., Hansen, B.T., Nolte, E., 1997. On the origin of saline fluids in the KTB (continental deep drilling project of Germany). Appl. Geochem. 12, 831–849.
McIntosh, J., Garven, G., Hanor, J., 2011. Impacts of Pleistocene glaciation on large-scale groundwater flow and salinity in the Michigan Basin. Geofluids 11 (1), 18–33.
Meinken, W., Stober, I., 1997. Permeability distribution in the Quaternary of the Upper Rhine glacio-fluvial aquifer. Terra Nova 9 (3), 113–116.
Montcoudiol, N., Molson, J., Lemieux, J.-M., 2014. Groundwater geochemistry of the Outaouais Region (Québec, Canada): a regional-scale study. Hydrogeol. J. 23, 377–396.
Nordstrom, D.K., Olsson, T., 1987. Fluid inclusions as a source of dissolved salts in deep granitic groundwaters: saline water and gases in crystalline rocks. Geol. Assoc. Can. 33, 111–119.
Nordstrom, D.K., Ball, J.W., Donahoe, R.J., Whittemore, D., 1989. Groundwater chemistry and water-rock interactions at Stripa. Geochim. Cosmochim. Acta 53, 1727–1740.
Parent, M., Occhietti, S., 1988. Late Wisconsinan deglaciation and Champlain sea invasion in the St Lawrence valley. Québec. Géogr. Phys. et Quat. 42, 215–246.
Pauwels, H., Fouillac, C., Fouillac, A.-M., 1993. Chemistry and isotopes of deep geothermal saline fluids in the Upper Rhine Graben: origin of compounds and water-rock interactions. Geochim. Cosmochim. Acta 57 (12), 2737–2749.
Pekdeger, A., Balderer, W., 1987. The occurrence of saline groundwaters and gases in the crystalline rocks of Northern Switzerland. Saline water and gases in crystalline rocks. Geol. Assoc. Can. 33, 127–143.
Piper, A.M., 1944. A graphic procedure in the geochemical interpretation of water-analyses Transactions. Am. Geophys. Union 25, 914–928.
Richard, S.K., Chesnaux, R., Rouleau, A., Morin, R., Walter, J., Rafini, S., 2014. Field evidence of hydraulic connections between bedrock aquifers and overlying

granular aquifers: examples from the Grenville Province of the Canadian Shield. Hydrogeol. J. 22, 1889–1904.
Rivers, T., Martignole, J., Gower, C.F., Davidson, A., 1989. New tectonic divisions of the grenville province, southeast canadian shield. Tectonics 8, 63–84.
Rouleau, A., Walter, J., Daigneault, R., Chesnaux, R., Roy, D.W., Germaneau, D., Lambert, M., Moisan, A., Noël, D., 2011. Un aperçu de la diversité hydrogéologique du territoire du Saguenay-Lac-Saint-Jean (Qc). Proceedings of GeoHydro 2011, Joint Meeting of the Can. Quat. Association, IAH Can. Chapter.
Roy, D.W., Beaudoin, G., Leduc É, Rouleau, A., Walter, J., Chesnaux, R., Cousineau, P., 2011. Post glacial differential isostasy in the Lac-Saint-Jean area (Qc) and implications for the quality of groundwater. Proceedings of GeoHydro 2011, Joint Meeting of the Can. Quat. Association, IAH Can. Chapter.
Simard, G., Des Rosiers, R., 1979. Qualité Des Eaux Souterraines Du Québec, MRN Dir. Gén. Eaux. (161p).
Statsoft Inc, 2013. STATISTICA (Data Analysis Software System) Version 12. Statsoft, Inc.
Stober, I., Bucher, K., 1999a. Deep groundwater in the crystalline basement of the Black Forest region. Appl. Geochem. 14 (2), 237–254.
Stober, I., Bucher, K., 1999b. Origin of salinity of deep groundwater in crystalline rocks. Terra Nova-Oxford 11 (4), 181–185.
Tóth, J., 1985. Role of regional gravity flow in the chemical and thermal evolution of ground water. First Can./Am. Conf. on Hydrogeology: Practical Applications of Ground Water Geochemistry.
Tóth, J., 1999. Groundwater as a geologic agent: an overview of the causes, processes, and manifestations. Hydrogeol. J. 7, 1–14.
Templ, M., Filzmoser, P., Reimann, C., 2008. Cluster analysis applied to regional geochemical data: problems and possibilities. Appl. Geochem. 23, 2198–2213.
Tremblay, G., 1971. Glaciation et déglaciation dans la région Saguenay-Lac-Saint-Jean, Québec, Canada. Cahiers de géographie du Québec 15, 467–494.
Walter, J., Rouleau, A., Clark, I.D., Guha, J., 2006. A First Investigation of Groundwater Geochemistry in the Crystalline Bedrock Around Lake Saint-Jean. Québec IAH Can. Chapter.
Walter, J., Rouleau, A., Roy Daigneault, D.W.R., 2011. Hydrogéochimie des eaux souterraines de la région du Saguenay-Lac-Saint-Jean: résultats préliminaires. In: Proceedings of GeoHydro 2011, Joint Meeting of the Can. Quat. Association. IAH Can. Chapter.
Walter, J., 2010. Les Eaux Souterraines à Salinité élevée Autour Du Lac Saint-Jean, Québec: Origines Et Incidences. Université du Québec à Chicoutimi: ix, Chicoutimi (177 p.).
Wigley, T., 1973. The incongruent solution of dolomite. Geochim. Cosmochim. Acta 37 (5), 1397–1402.
Woussen, G., Martignole, J., Nantel, S., 1988. The Lac-St-Jean anorthosite in the St-Henri-de-Taillon area (Grenville Province): a relic of a layered complex. Can. Mineral. 26, 1013–1025.